Article:
Stevenson, R. and Bowman, E. (2025) Effective stress and suffusion onset at local and global scales in centrifuge permeameter tests. Journal of Geotechnical and Geoenvironmental Engineering, 151 (2). 04024162. ISSN: 1090-0241

https://doi.org/10.1061/jggefk.gteng-13169

Effective Stress and Suffusion Onset at Local and Global Scales in Centrifuge Permeameter Tests

Rowena Stevenson, Ph.D.[1] and Elisabeth Bowman, Ph.D.[2]

[1]Research Associate, Department of Civil and Environmental Engineering, Imperial College London, London, SW7 2AZ, U.K. (corresponding author). ORCID: https://orcid.org/0000-0002-3821-8529. Email: rowena.stevenson@imperial.ac.uk

[2]Reader, School of Mechanical, Aerospace and Civil Engineering, University of Sheffield, Sheffield, S1 3JD, U.K. ORCID: https://orcid.org/0000-0001-7868-6688. Email: e.bowman@sheffield.ac.uk

ABSTRACT

This study presents the results from a series of centrifuge tests conducted in a novel permeameter capable of measuring both global and layer permeability. Six tests were undertaken at gravitational accelerations ranging from 10- to 40-g. Using a parametric modelling approach, the research examines the influence of effective stress gradient on the onset and progression of suffusion in an under-filled, gap-graded soil. At a specimen scale, increased effective stress gradient appears to increase suffusion susceptibility in identically prepared models. However, analysis of the permeability response of individual layers indicates that initial microscale variability and hydraulic loading history have arguably more impact on the suffusion behaviour than effective stress. At the layer scale, suffusion and clogging events occurred from the onset of seepage flow and there was no observed influence of effective stress level on suffusion onset. The study finds that the definition of suffusion onset is highly dependent on experimental design, and critically evaluates the concept of threshold hydro-mechanical conditions for suffusion onset.

INTRODUCTION

The seepage of water through earth structures such as embankment dams and levees can lead to internal erosion, a process responsible for almost 50% of historical failures (Foster et al. 2000). This paper focuses on suffusion, one of the four types of internal erosion identified by ICOLD (2017). Suffusion is defined as the selective erosion of the finer soil particles of an under-filled, gap-graded soil under the action of seepage flow and is characterised by no volumetric change of the soil. This leads to an increase in permeability, causing unexpectedly high flow-rates through a structure to develop over time. Migrated particles may also be redeposited in a process termed "clogging", altering the hydraulic regime and potentially causing global failure of the structure. Despite being a well-acknowledged problem, the factors controlling suffusion erosion are not fully understood. However, it is generally accepted that suffusion potential is governed by the geometric stability of the material, with suffusion occurring when a critical combination of hydraulic and stress conditions is reached within the soil (Garner and Fannin 2010).

Geometric instability criteria, such as those from Kezdi (1979) and Kenney and Lau (1985), assess suffusion potential based on particle size distribution. Using such criteria, Skempton and Brogan (1994) observed that suffusion onset under upwards flow occurred in internally unstable soils at hydraulic gradients below Terzaghi's conditions for heave. They termed this onset point the "critical hydraulic gradient", i_{cr}. Subsequent studies have characterized this threshold. Notably, the experimental studies of Li (2008) led to the development of a hydromechanical envelope concept, where the critical hydraulic gradient is taken to be a factor of both the effective stress in the soil and the seepage path length. The most recent formulation of this critical hydraulic gradient for downwards flow is given by Eq. 1, from Li and Fannin (2022), where α is the stress reduction factor from Skempton and Brogan (1994) and σ'_{vm0} is the mean vertical effective stress for the soil element under hydrostatic conditions normalised by the unit weight of the water, γ_w, and the seepage path length, Δz.

$$i_{cr} = \frac{\alpha}{1-\alpha}\left(\frac{\sigma'_{vm0}}{\gamma_w \Delta z} + 0.5\frac{\gamma_s - \gamma_w}{\gamma_w}\right) \tag{1}$$

Ke and Takahashi (2014) also found that increasing effective stress increased i_{cr} in their rigid-walled permeameter tests carried out on gap-graded soils (fines content between 15 % and 35 %. Liang et al. (2019) also found this relationship for tests undertaken on a 20 % fines soil under different isotropic stresses. Later works in the same permeameter as Li (2008) somewhat contradict the effective stress influence suggested by Eq. 1, with both Crawford-Flett (2014) and Slangen (2015) finding that for an under-filled (<20% fines content) material – Li (2008) used both under-filled and transitional soils (20-36% fines) – suffusion onset was completely independent of effective stress. Triaxial stress states have been shown to either increase or decrease i_{cr}, depending on the direction of the major principle stress in relation to the seepage flow direction (Chang and Zhang 2013).

Stress state also influences the progression of suffusion, with Bendahmane et al. (2008) observing double the maximum erosion rate in specimens at a confining stress of 100 kPa compared to 150 kPa in a flexible-walled permeameter study. In a rigid-walled permeameter study, Rochim et al. (2017) found that internally unstable specimens subjected to more rapid hydraulic loading exhibited significantly more fine particle loss compared to those loaded gradually. Early permeability variations indicated significant fines migration within the specimen before external suffusion was observed.

The seepage path length term, Δz, is included in Eq. 1 because of the significant difference in i_{cr} that Li (2008) observed for the same glass bead gradation in two different sized permeameters, with i_{cr} being seven times larger in the smaller (102 mm diameter) compared to the larger (279 mm diameter) permeameter. Zhong et al. (2018) also found that i_{cr} decreased with Δz when using two different sized permeameters, although the two tests had very different boundary conditions, as the smaller cell had flexible walls, whilst the larger was a rigid-walled apparatus.

Both the effective stress conditions and seepage path length influence suffusion, but the variety of boundary conditions - even within the same study - makes this difficult to quantify. Scaling relationships in centrifuge modelling can potentially minimise these issues by replicating diverse stress conditions within one experimental set-up. The limited use to date of centrifuge testing to explore this problem is likely due to the complexity of scaling crucial internal erosion parameters, including hydraulic and pressure gradients (Ovalle-Villamil and Sasanakul 2020). The only previous centrifuge suffusion study was undertaken by Marot et al. (2012), testing a sand/kaolin mixture with 10 % fines content and gap ratio of around 30 under constant head downwards flow at g-levels between 10- and 40-g. That parametric study, which varied both the applied head difference and specimen length, found that doubling the length of the specimen reduced i_{cr} by 40 % and doubled the rate of erosion. The critical hydraulic gradient was identified by the first presence of fines in the effluent water and pore pressures were measured across the whole sample.

This study presents the results of a series of multi-stage, downward seepage flow tests undertaken on a dense, gap-graded, under-filled soil in a novel centrifuge permeameter. The test arrangement allowed a significant effective stress gradient to be imposed across the specimen, and interstitial pore pressure readings facilitated both layer-wise and global permeability analysis. The suite of tests was designed to explore the influence of effective stress on the onset and progression of suffusion using a parametric modelling approach. The spatial and temporal development of suffusion within the six tests, conducted at accelerations between 10- and 40-g, is presented, and the concept of a threshold value for the onset of suffusion is critically examined.

CENTRIFUGE TESTING

Centrifuge testing is widely used to represent real-scale (prototype) stress conditions in relatively small models by accelerating them to many times Earth's gravity. Whilst the stresses and pressures between the model and prototype are the same, other properties are scaled with the centrifuge acceleration factor, N. In problems with complex geometries or multiple interacting processes such as suffusion, the scaling laws are not immediately apparent. In this case, a parametric modelling approach can be taken to better understand the fundamental mechanisms in process. The scaling laws relevant to suffusion are summarised in Table 1, where a scaling factor of N indicates that the parameter is N times larger for the prototype compared to the model. The grain size is conventionally not scaled as the soil material is assumed to have the same stress-strain relationship at the continuum level (Taylor 1994).

As indicated by the † symbol in Table 1, the scaling relationships related to Darcy's Law are somewhat contested. Both i and k are macroscale parameters, with i representing a decrease in total fluid head across the length of a seepage path and k being a function of both the soil structure and properties of the permeant fluid. In the centrifuge, when the fluid and soil are kept constant, the permeability, k, scales with g-level (Garnier et al. 2007). The hydraulic gradient is dimensionless and does not scale, leading to the seepage velocity, v, scaling by N. In the only previous suffusion study undertaken in the centrifuge by Marot et al. (2012), a factor of N was applied to the hydraulic gradient, as the head difference across the sample was scaled but not the model height. This approach is not consistent with standard centrifuge scaling practice, where the soil is considered as a continuum.

In reality, hydraulic gradient is a macroscale parameter based on hydraulic head which is used to express the energy loss across a sample due to elevation change and frictional losses. In 1-g suffusion testing, the change in hydraulic gradient is used as convenient, easy-to-calculate parameter which quantifies the change in permeability caused by work done in the migration of fine particle within the microscale granular structure of the soils. In the centrifuge, this relationship breaks down due to the scaling factors related to lengths compared to stresses and energy. Consequently, this study uses the change in potential energy gradient, EG, across the model in place of i to capture the suffusion process. This is based on the modified Darcy's law from Thusyanthan and Madabhushi (2003) to calculate the 1-g permeability of a soil, k_{1g}, from centrifuge permeameter tests shown in Eq. 2, where v is Darcy's seepage flow velocity for laminar flow, k_{1g} is Darcy's permeability at 1-g, γ_{1g} is the unit weight of the fluid at 1-g. ΔP is the pore pressure difference across a length, ΔL, in the direction of seepage and $\Delta z \rho N g$ is the elevation pressure difference across same length in the centrifuge. This approach captures the fact that there is greater energy dissipation over the same granular matrix at the microscale for an identical model tested at a higher g-level, whilst the hydraulic gradient would be the same for both as the ratio between the prototype length and pressure gradient stays constant.

$$v = \frac{k_{1g}}{\gamma_{1g}} \times \frac{\Delta \left(P + z\rho Ng\right)}{\Delta L} = \frac{k_{1g}}{\gamma_{1g}} \times EG \tag{2}$$

The gravitational acceleration Ng is a function of the angular velocity of the centrifuge, ω, and its radius, R. For each test, a single N value is quoted based on an effective radius representative of the model, but due to the relatively small radius of the centrifuge in comparison to the radius of the Earth, N can vary significantly across the height of a model. This can be corrected for when analysing the test data. It is not appropriate to consider the elevation head at the top of the sample as just the length of the seepage path, rather, as shown in Eq. 3, Anderson et al. (2015) formulates it as a potential energy difference across a model height, $P\left(d\right)$, at any distance from the datum, d, where r_b is the radius to the base of the sample. In a similar way, the non-linear variation in effective stress across the model height can also be accounted for, shown in Fig. 1a.

$$P\left(d\right) = \rho\omega^2 \left(r_b d - \frac{d^2}{2}\right) \tag{3}$$

Testing device

Although some suffusion work has previously been undertaken in the centrifuge environment by Marot et al. (2012), the centrifuge permeaeter presented in this study represents a significant advancement in testing capabilities, with the addition of interstitial pore pressure measurement ports and multi-stage hydraulic loading. The experimental apparatus resembles a typical 1-g constant head rigid-walled permeameter setup, slightly modified for the centrifuge environment.

Fig. 2a shows the payload installed on the 2 m radius 50 g-ton beam centrifuge at the University of Sheffield. The de-aired water for the test is stored in a pressurised container (A in Fig. 2a) which feeds an upstream constant head tank (CHT). This tank (B) is fixed in place and a pore pressure transducer (PPT) is installed in its base to monitor the water level during testing. The cell (C) sits in the middle of the payload with seven PPTs along the side wall (D), allowing the specimen to be considered in six discrete layers. The head difference applied to the specimen is controlled by lowering the downstream CHT (E) incrementally, creating downward seepage flow conditions.

The flow rate is measured by recording the height of water in the straight-sided outflow container (F) using a further PPT (G) in the base. A GoPro camera (H) taking pictures every 60 seconds is trained on the specimen to monitor any soil settlement, which was not observed in any of the tests in this study.

The permeameter cell, Fig. 2b, consists of a top and bottom cap and stacked acrylic cylinders, sealed against each other by internal O-rings, greased by silicon grease, and held together with steel tie rods. The cell has an internal diameter of 77 mm and 7 PPT ports are located at 35 mm intervals along the side wall, allowing specimens up to 210 mm in height to be tested. All PPTs used in the apparatus are model EPB-PW from StrainSense Ltd. with a 350 kPa range and a 6 µm porous ceramic filter (air entry value 0.5 bar). The PPTs have a diameter of 6.4 mm and length of 11.4 mm. Each sensor in the cell is fitted flush with the internal wall and sealed in place with an O-ring.

Using stacked cylinders allows for shorter samples to be tested by using only two or three of the four cylinders, as needed. During a test, the water enters the reservoir in the top cap of the cell, via a perforated acrylic disk and through a coarse, free-draining overburden soil (Leighton Buzzard fraction A, LB-A, shown in Fig. 3). The base of the cell includes a conical outflow to avoid clogging and is also filled with LB-A. This coarse soil has a particle size distribution chosen to allow free passage of migrating fines whilst providing support for the coarse matrix of the specimen. This solution was reached after initial trials with increasingly coarse filter meshes. The results of these trials raised concerns of clogging in the very bottom layer of the specimen due to the harsh transition between soil and free space, and so a granular filter was used, similar to those used in practice in water-retaining structures.

Materials

For this study, a gap-graded (gap ratio $D'_{15}/d'_{85} = 3.33$) under-filled (20% fines) soil mix is used. The α factor concept of Skempton and Brogan (1994), suggests that the effective stress applied to this soil mix will therefore be transferred by the matrix of coarse particles, with the fine particles sitting unstressed in the void spaces. To ensure that laminar flow requirements are met in the centrifuge environment, a typical unstable sand/gravel mix has been scaled down to a silt/sand mix, whilst preserving the shape of the particle size distribution (PSD), on which most instability criteria are based. For the coarser fraction, uniformly graded HST95 Congleton silica sand is used, with particles less than 90 µm in diameter removed by sieving prior to testing to create a clear gap between the coarse and fine fractions. HIM2 silica flour (silt) is used to represent the finer fraction. Fig. 3 gives the PSD of the unstable mix alongside the PSDs for the constituent fractions and the coarse overburden soil (LB-A). The inset table gives key soil parameters. The final soil mix is unstable according to the most common geometric criteria of (Kezdi 1979; Kenney and Lau 1985; Li and Fannin 2008; Wan and Fell 2008), with a minimum H/F value of 0.609.

Specimen preparation

Small batches of soil mix were prepared by mixing the sand and silt in a 4:1 ratio with water to reach a 5 % water content and sealed in an airtight plastic bag for 16 hours to promote moisture homogeneity. To begin specimen preparation, LB-A sand was dry-pluviated to 5 mm below the lowest PPT. The specimen was prepared on top of this in 15 mm layers to achieve a relative density of 70 % (void radio $e = 0.58$) using the moist-tamping procedure from Ladd (1978) to avoid excessive segregation. Once the desired model height was reached, the rest of the cell was filled with LB-A sand to provide the required overburden stress.

Carbon dioxide was percolated through the sample from the base for 20 minutes to displace the air. The sample was then saturated with de-aired water under upwards flow at 600 mm^3/min, allowing at least one pore volume of water to flush through the sample. No suspended fines were observed in the effluent water. The cell was then installed on the centrifuge beam for testing.

Testing programme

In total, six downwards flow permeameter tests were undertaken at between 40- and 10-g. The test naming convention identifies first the g-level (40/30/20/10), followed by the model height (L for full-height, S for half-height), and the increment that the downstream CHT was lowered for each step (between 2.5 and 10 mm). The repeat of test T40L2.5 is identified by the suffix (R). Table 2 gives a comprehensive overview of the test conditions for each test, with the hydraulic loading regimes shown in Fig. 1b. The half height test T40S2.5 has been included as it has the same effective stress gradient as T20L5 but with a shorter model height (Fig. 1a).

To begin a test, the upstream and downstream CHTs (B and E in Fig. 2a) were level and there was no flow. The centrifuge was accelerated to the target g-level and held for a few minutes to establish the hydrostatic pore pressure profile. To begin downwards seepage flow, the downstream CHT was lowered by one increment, dh_{CHT}. This increment was chosen to apply approximately the same change in applied energy gradient ($\Delta EG_{app} \approx 4\,\mathrm{kPa/m}$) in the early stages of testing for tests at different g-level, with dh_{CHT} varying from 2.5 mm at 40-g to 10 mm at 10-g. For T30L2.5/5, an average increment of 3.75 mm was achieved by alternating increments of 2.5 mm and 5 mm due to the limitations of the stepper motor, which was restricted to 25 mm increments. Each increment was held for a desired duration (typically 120 s) and then the downstream CHT was lowered again. In T10L10, the increments had a longer duration of 600 s to ensure the volume of water through the cell was large enough to capture the slower flow rate in the outflow container.

The limited capacity of the outflow container meant that tests had to be conducted in several stages, between which the centrifuge was spun down. The CHTs were kept level, meaning the downwards flow regime was preserved, although at a much lower flow rate, throughout the break. Deceleration followed a pattern of decreasing increments of 10-g, with each increment being held for a few seconds. After the adjustments were made at 1-g, the centrifuge was accelerated up to the target g-level in increments of 10-g held for 10 seconds each. This reduction and then increase in stress conditions had some, albeit limited, impact and is discussed in a later section. The number of stages for each test (between 2 and 4) is given in Table 2. The points of spin-down are indicated with coloured arrows in the hydraulic loading regimes shown in Fig. 1b, as well as in the permeability results presented in Figs. 5 and 6. The tests concluded when the desired applied energy gradient, EG, across the specimen had been reached.

RESULTS

Defining a suffusion event

At least some of the variation in reported suffusion responses between studies must be attributed to the variation in definition of suffusion onset. Zhong et al. (2018) defined onset as a 10 % permeability change measured across an interval, whilst Li (2008) looked for a seepage velocity change and rapid increase in permeability. In this study, a suffusion event is classified as a period in which a specimen layer increases in permeability, assumed to be due to the loss of fines, calculated by the pore pressure difference between adjacent PPT ports. To isolate suffusion events from background noise and small PPT fluctuations and facilitate comparison between the tests, the following four criteria must be met for a suffusion event to be identified:

- The suffusion event must have a duration longer than 120 seconds
- The permeability must increase by at least 1×10^{-6} m/s over the event
- Any slight decreases in permeability must last less than 30 seconds and permeability must not drop below the value at the start of the event
- The suffusion event ends at the point before the permeability begins to decrease or plateau for longer than 30 seconds

These criteria do not quantify the rate or magnitude of erosion and some suffusion events see the permeability increase by significantly more than the lower limit. These events are indicated in the timeline at the bottom of the layer permeability figure for each test. The definition of suffusion onset used in this study is more similar to Zhong et al. (2018) corresponding to a permeability increase of ~5 % over two minutes. This is likely in part why suffusion was observed at significantly lower hydraulic gradients compared to Li (2008).

Global permeability

Fig. 4 shows the global permeability profiles of the specimens over the testing duration. All permeabilities in this study are given as 1-g permeabilities, calculated using Eq. 2. Flow rate and pore pressure data for each centrifuge test are presented in Figs. S1-S12 in the Supplemental Materials. There was some variation in the initial permeabilities of the specimens, ranging between

1.43×10^{-5} m/s and 2.85×10^{-5} m/s. This must be attributed to sample preparation, although spatial particle size analysis of a typically-prepared specimen after saturation and before erosion showed a fines content of 20% ± 0.2% along the specimen height (Stevenson 2024). A 1-g falling head permeameter test (Head 1982) on the same soil gave a permeability of 1.63×10^{-5} m/s, agreeing well with the starting centrifuge k_{1g} values.

There is a clear difference between the response of specimens tested at higher g-levels, compared to the lower g-levels. For tests at 40-g, all of the specimens exhibit global suffusion, as they all showed a net increase in permeability over the duration of the test, as shown in Table 2. Test T30L2.5 exhibits three suffusion events over the test duration, despite the net decrease in permeability from the beginning to the end of the test. In contrast, tests T20L5 and T10L10 showed a continual decrease in permeability over the test duration. This decrease suggests that some fines migration was occurring within the specimens, but no global suffusion event was observed. In general, there was more fluctuation in permeability towards the start of the tests, with specimens switching more rapidly between suffusion and clogging behaviour at higher g-levels. By the end of testing, most tests showed a gradual clogging behaviour, with the exception of test T10L10, which reached a constant permeability after around 90 minutes of seepage flow.

Layer permeability

Whilst global permeability gives an overview of the specimen behaviour, the permeability of each layer gives a more detailed understanding of the spatial and temporal initiation and development of suffusion and clogging within a specimen. Figs. 5 and 6 show the layer permeability profiles for each test in this study, with suffusion events, as previously, indicated on the timeline at the base of the figure. In the following section, notable results for the full-height tests are discussed in order of decreasing g-level (N value), followed by the shorter sample, T40S2.5.

In Fig. 5a, the results for T40L2.5 show that all layers of the specimen experience suffusion events from almost the first onset of seepage flow. There is a trend of shorter, more pronounced suffusion events happening in the lighter-stressed upper layers at the start of the test, transitioning to longer, more gradual, increases in permeability towards to bottom of the specimen during Stage

2 and the early part of Stage 3. By the end of testing there is very little permeability fluctuation anywhere within the specimen. A similar observation can be made for the repeat test T40L2.5(R) in Fig. 5b, where there is only one small suffusion event in Layer 1 during the later stage of testing. Unlike the short, sharp suffusion events observed in T40L2.5, the top layer of T40L2.5(R) experiences a suffusion event that continues from almost the start of testing to 50 minutes into seepage flow. There is much less fluctuation between suffusion and clogging within the layers.

The permeability of the layers of T30L2.5/5, shown in Fig. 6a, show less fluctuation than T40L2.5, although suffusion is still observed in all layers within the first two increments of applied head difference. In T20L5 only the topmost Layer 1 and the bottom two layers experience suffusion events, with Layers 2 and 3 clogging throughout (Fig. 6b). These layer-scale suffusion events are not captured in the continuously clogging global permeability profile. There is no layer-scale suffusion in the second stage of testing.

T10L10 shows a similar trend, with suffusion occurring predominantly in the top-most and bottom-most layers during the first stage (Fig. 6c). Unlike T20L5, there is some gradual suffusion during Stage 2. The abnormally high permeability readings from Layer 2 at the start of Stage 1 suggest that soil is not sufficiently compacted against the side wall, with local collapse of the granular matrix potentially explaining the stabilisation of this reading further into testing. As any observed increases in permeability are likely not due to suffusion events, this layer was excluded from further analysis.

The half-height test, T40S2.5, exhibits a very different behaviour to the other tests conducted at 40-g. Fig. 5c shows that suffusion occurs in all three layers within the first 52 minutes of testing, followed by continuous clogging. For this test, unlike the others in this study, the global permeability response is reasonably similar to the permeability profiles of the layers.

DISCUSSION

Repeatability

The repeatability in this study is validated by comparing the results of T40L2.5 and T40L2.5(R), which were prepared in an identical manner and subject to the same hydraulic loading regime. The repeat test, T40L2.5(R), was taken to a higher EG_{app}, 195.6 kPa/m compared to 236.5 kPa/m . It also comprises of two spin stages, compared to the three shorter stages for T40L2.5.

The permeability profiles for T40L2.5 and T40L2.5(R) in Fig. 4 show remarkable similarity, with the tests starting at 1.43×10^{-5} m/s and 1.60×10^{-5} m/s respectively. Both tests show an initial increase in permeability to around 2.1×10^{-5} m/s, reaching their most permeable after between 70 and 80 minutes of seepage flow testing. Both tests then exhibit gradual clogging at very similar rates for the remainder of the test. There is some variation in behaviour at the start of the test, with an abrupt global suffusion in the first 15 minutes of T40L2.5 which is not observed in the repeat test.

On a more local scale, shown by the layer graphs in Figs. 5a and 5b, there is more variation between the tests, likely due to the inherent particle-scale differences between identically prepared experimental models. However, a general trend can be observed. The top two layers, Layers 0 and 1, experience significant suffusion at low applied head differences earlier into the test, whilst the lower, more highly stressed layers tend to clog until higher applied energy gradients.

In the permeameter tests of Li (2008), suffusion appeared to initiate in random locations, presumed to be at a local defect or variation in the granular micro-structure. In this study which, unlike Li (2008), has a significant stress gradient across the specimen height, suffusion occurs at lower hydraulic loading in the more lightly stressed upper layers, at the start of the seepage path. At the scale of measurements taken in this study, the comparison of tests T40L2.5 and T40L2.5(R) shows that suffusion and clogging behaviour is replicated between the centrifuge permeameter experiments at both the specimen and layer scale.

Influence of spin-down breaks during testing

The centrifuge spin-down breaks, which were necessary for the recording of the flow rate during testing, meant a relaxation and subsequent reapplication of effective stress on the specimens, an effect that is more pronounced at higher g-levels. Over these breaks, the global permeability of the specimens tended to either remain constant or slightly increase. There is no clear relationship between the size of permeability increase and the magnitude of effective stress relief.

Comparison of the global and layer permeabilities show that global increases across a spin-down break are usually due to a larger increase in permeability in just one of the layers. This suggests a local internal rearrangement fines, perhaps close to the PPT port, that may not be representative of the whole layer. The maximum change in global permeability across a spin down break was +16 % between Stage 2 and 3 in T40L2.5.

Threshold conditions for the onset of suffusion

Fig. 7 takes all of the suffusion events identified in the specimen layers and plots the energy gradient across that layer against the effective stress at the midpoint of the layer at the point of suffusion onset. The first suffusion event in a particular layer is identifiable by a fully opaque marker, with later suffusion events appearing more faded. The hydromechanical envelope of Li and Fannin (2022) suggests that the onset of suffusion should occur at higher applied energy gradients in more highly stressed layers, assuming that the specimen is prepared homogeneously and no particle migration occurs before the onset of suffusion. Fig. 7 shows that many of the layers first experience suffusion at layer energy gradients below 10 kPa/m, essentially at the onset of seepage flow. There is no relationship between the mean effective stress level in an individual layer and the energy gradient at the onset of suffusion in the layer. For the under-filled, gap-graded material tested in this study, this layer-wise outcome is consistent with the theoretical α-factor interpretation of Skempton and Brogan (1994), as the fine particles are not considered part of the force-carrying matrix and so effective stress does not influence their suffusion. This interpretation only addresses the onset of suffusion and not its progression through the soil matrix. A different response is anticipated in over-filled suffosive soils, where fine particles are part of the force network, underscoring the need for further studies across a broader range of soil types.

The identification of suffusion onset is heavily influenced by both the researcher's definition of suffusion and the experimental design, potentially explaining the discrepancy between the findings of existing studies. The definition of a suffusion event has been explicitly stated in this study, and is similar to the criteria defined by Zhong et al. (2018). Other studies consider suffusion to occur when there are visible fines in the effluent, or the flow rate increases dramatically. By either of these criteria, suffusion would not be identified in the specimens in this study, despite the observed increases in permeability. The concept of a critical hydraulic (or energy) gradient is predicated on the idea that one area reaches the threshold conditions and then erodes so much that the flow rate through the whole sample increases, but for this to happen there must have already been significant rearrangement of fine particles within the specimen.

The results of this study show that particle migration occurs from the onset of seepage flow in internally unstable soils, which has been captured by taking layer permeability readings in this study. The specific effective stress and hydraulic loading conditions governs whether this local rearrangement progresses to become observable suffusion or clogging mechanisms, or if it self-stabilises at a scale smaller than the finest experimental measurement points. This local rearrangement introduces a history element which explains why layers of different models at the same effective stress in Fig. 7 do not begin to erode at the same energy gradient.

Parametric modelling

In this section, the centrifuge test results are analysed using a conventional continuum-based parametric approach. While continuum-based threshold criteria, like the critical hydraulic gradient, should theoretically be consistent for models under identical prototype conditions, suffusion is inherently non-homogeneous across a specimen. The following sections underscore the limitations of using global parameters to accurately quantify suffusion.

T40S2.5 and T20L5

Tests T40S2.5 and T20L5 aimed to replicate the same prototype, assuming standard continuum centrifuge scaling laws. Ostensibly this would suggest that they are governed by the same hydro-mechanical envelope for the onset of suffusion, but comparison of their global permeability profiles in Fig. 4 reveals very different responses to the hydraulic loading. The 40-g half-height test, T40S2.5, experienced three significant suffusion events during testing, with the most significant being an increase of 2.17×10^{-6} m/s over 12 minutes, starting at an applied energy gradient of 61.5 kPa/m. In contrast, despite having a similar effective stress profile across the specimen height (Fig. 1a) and reaching the same hydraulic conditions as T40S2.5, the full height T20L5 did not experience global suffusion.

From a centrifuge scaling perspective, these two tests have the same prototype specimen height when considering the soil as a continuum. Tests undertaken at 1-g have conventionally taken the specimen height to be analogous to the seepage path length and used it to formulate hydro-mechanical criteria. Within the centrifuge, it is clearly not appropriate to make this assumption, as suffusion is intrinsically a local granular phenomenon. Specimens T40S2.5 and T20L5 do not have the same granular structure in terms of the ratio of particle size to seepage path length, and consequently number of pore constrictions that eroding particles must migrate through. This, in part, accounts for the difference in their responses during this study.

T40L2.5, T30L2.5/5, T20L5 and T10L10

Comparing the results of these four identically prepared models tested between 10- and 40-g demonstrates that the hydro-mechanical loading regime has a significant impact on the suffusion response of the specimen. Notably, test T40L2.5 exhibited suffusion from the onset of seepage flow, while T30L2.5/5 demonstrated suffusion some time into testing. This contrasts with the tests under smaller effective stresses, T20L5 and T10L10, which consistently clogged throughout. This suggests that specimens subject to higher effective stress may be more susceptible to suffusion, a conclusion which may have concerning real-life implications. This finding diverges from previous studies, which observed that a higher effective stresses either increases (Li 2008; Ke and Takahashi 2014; Liang et al. 2019) or does not affect i_{cr} (Crawford-Flett 2014; Slangen 2015).

However, it may not be solely the effective stress conditions that has led to the difference in response between these tests, as they had different hydraulic loading regimes. In both tests T40L2.5 and T30L2.5/5, the first global suffusion events occurred at an applied energy gradient of approximately 7 kPa/m. Despite the final applied energy gradients for both T20L5 and T10L10 being significantly greater than these values, no global suffusion was observed in these lower g-level tests. The maximum seepage velocity in both tests T20L5 and T10L10 also reached the values observed at the onset of suffusion in tests T40L2.5 and T30L2.5/5, although the velocity increased at a slower rate due to the smaller N value. This indicates that there is a significant impact of the hydraulic loading history on the progression of suffusion, with more gradual increase in seepage velocity potentially having an initially stabilising influence.

A more gradual loading regime was found by Rochim et al. (2017) to cause initial clogging, followed by a significant increase in global permeability. In both this study and Rochim et al. (2017), this initial clogging behaviour indicates some local migration of fine particles. This can be seen by comparing the layer permeability profiles in Figs. 5 and 6. Short, sporadic suffusion events occurred in both T20L5 and T10L10 during the first few hydraulic loading increments, whilst longer, more gradual increases in layer permeability were observed towards the end of the tests. This general trend was the same between all four tests compared here, suggesting that the incremental onset of very low seepage flow causes an initial rearrangement of fine particles, but a higher hydraulic loading is needed to cause continuing suffusion to occur. When comparing the behaviour of the interstitial layers of these four specimens there was greater fluctuation in permeability in the higher g-tests, which had larger increments of applied energy gradient. This suggests a more dynamic formation of zones of suffusion or clogging locally under higher hydro-mechanical loading.

Whilst the relatively long specimen length in this test arrangement allows the spatial development of suffusion to be observed, the interstitial PPTs allow for an alternative approach to be taken. Focusing on the top 35 mm layer of each test isolates the influence of effective stress and layer permeability. The two top layers with lower initial k_{1g}, T40L2.5 and T10L10, eroded from almost the start of the test, despite being at completely different effective stress levels. In contrast, the top layers with higher initial k_{1g}, T30L2.5/5 and T20L5, began by decreasing in permeability, only later experiencing suffusion events. These decreases in k_{1g} must be due to local fines rearrangement within the layer, as no new particles can enter the top layer from above and there was no recorded settlement of these dense specimens in any of the tests. Hence, the local permeability due to variations in specimen preparation seems to be significantly more influential than the effective stress state in these tests.

According to Eq. 1, all of the top layers have calculated i_{cr} between 11.6 and 16.0, equivalent to EG upwards of 1×10^3 kPa/m. However the layers experience suffusion events at energy gradients between 8 kPa/m and 20 kPa/m. This value is similar to just one of the hydraulic loading increments in Li (2008), which were around $i = 1$ or $EG = 9.8$ kPa/m. Fundamentally, the concept of critical hydraulic gradient is based on one zone of a specimen reaching a hydraulic condition which is enough to instigate the migration of fine particles. However the only way to build up hydraulic gradient locally is to change the inter-particle network of the soil. In dense under-filled soils in particular, where settlement of the granular matrix is unlikely, this local increase in hydraulic gradient can only occur due to the deposition of particles from further upstream by the seepage flow. In which case, internal fines migration must be occurring before the critical value that is implied by hydromechanical frameworks such as Eq. 1.

CONCLUSIONS

This paper presents the results of a series of multi-stage suffusion tests in a novel centrifuge permeameter that allows both global and layer-wise permeability measurements. The results showed very good repeatability in the new apparatus. Specimens with a greater effective stress gradient along the specimen height exhibited global suffusion, whilst lower-stressed specimens decreased in permeability, contrary to some previous studies. However, examining the response of individual layers reveals a more complex spatial and temporal particle migration behaviour within the specimens that is not captured by the global permeability, bringing into question the definition of suffusion onset.

All centrifuge tests showed layer-scale migration of fine particles even at low hydraulic loading. These suffusion and clogging events were not reflected in the global permeability reading. There was no relationship between the mean effective stress within the individual layers and the energy gradient at the onset of suffusion in that layer. The results do no fit into the concepts, such as critical hydraulic gradient, that are based on a threshold condition for suffusion onset.

Although specific to one under-filled, gap-graded soil gradation, this study shows that permeameter tests cannot be considered element tests for suffusion, as particle migration is not homogeneous, even across relatively small samples. Hydraulic loading history and initial granular variability within the specimen have arguably more impact on both suffusion initiation and progression than effective stress. The choice of measurement locations and methods, as well as the definition of a suffusion event, are crucial to robust experimental design in this field, and should be considered thoroughly in future studies.

DATA AVAILABILITY STATEMENT

Some or all data, models, or code that support the findings of this study are available from the corresponding author upon reasonable request

SUPPLEMENTAL MATERIALS

Figs. S1–S12 are available online in the ASCE Library (ascelibrary.org).

Acknowledgments

The first author was supported by an Engineering and Physical Sciences Research Council (EPSRC) DTA Scholarship. We are grateful for the assistance of the technicians of the Department of Civil and Structural Engineering at the University of Sheffield and in particular Alex Cargill for construction of the permeameter apparatus.

REFERENCES

Anderson, C., Sivakumar, V., and Black, J. A. (2015). "Measurement of permeability using a bench-top centrifuge." *Géotechnique*, 65(1), 12–22.

Bendahmane, F., Marot, D., and Alexis, A. (2008). "Experimental parametric study of suffusion and backward erosion." *J. Geotech. Geoenviron. Eng.*, 134(1), 57–67.

Chang, D. S. and Zhang, L. M. (2013). "Critical hydraulic gradients of internal erosion under complex stress states." *J. Geotech. Geoenviron. Eng.*, 139(9), 1454–1467.

Crawford-Flett, K. (2014). "An improved hydromechanical understanding of seepage-induced instability phenomena in soil." Ph.D. thesis, University of British Columbia, Vancouver, Canada.

Foster, M., Fell, R., and Spannagle, M. (2000). "The statistics of embankment dam failures and accidents." *Can. Geotech. J.*, 37, 1000–1024.

Garner, S. J. and Fannin, R. J. (2010). "Understanding internal erosion: a decade of research following a sinkhole event." *Hydropower and Dams*, 17(3), 93–98.

Garnier, J., Gaudin, C., Springman, S. M., Culllingan, P. J., Goodings, D., Konig, D., Kutter, B., Phillips, R., Randolph, M. F., and Thorel, L. (2007). "Catalogue of scaling laws and similitude questions in geotechnical centrifuge modelling." *Int. J. Phys. Model. Geotech.*, 3, 1–23.

Head, K. H. (1982). *Manual of Soil Laboratory Testing Volume 2: Permeability, shear strength and compressibility tests*. New York: Halsted Press, 2 edition.

ICOLD (2017). "Internal erosion of existing dams, levees and dykes, and their foundations." *Bulletin 164, Volume 1: Internal Erosion Processes and Engineering Assessment*, J. J. Bridle, R. Fry and R. Fell, eds., Paris, International Commission on Large Dams.

Ke, L. and Takahashi, A. (2014). "Experimental investigation on suffusion characteristics and its mechanical consequences on saturated cohesionless soil." *Soils. Found.*, 54, 713–730.

Kenney, T. C. and Lau, D. (1985). "Internal stabilities of granular filters." *Can. Geotech. J.*, 22(2), 215–225.

Kezdi, A. (1979). *Soil physics: selected topics (developments in geotechnical engineering)*. Elsevier Science Ltd., 1st edition.

Ladd, R. (1978). "Preparing test specimens using undercompaction." *Geotech. Test. J.*, 1(1), 16–23.

Li, M. (2008). "Seepage induced instability in widely graded soils." Ph.D. thesis, University of British Columbia, Vancouver, Canada.

Li, M. and Fannin, R. J. (2008). "Comparison of two criteria for internal stability of granular soil." *Can. Geotech. J.*, 45, 1303–1309.

Li, M. and Fannin, R. J. (2022). "Internal erosion: critical hydraulic gradient in one-dimensional vertical seepage and its relation to soil gradation." *Can. Geotech. J.*, 59(5), 769–772.

Liang, Y., Yeh, T.-C. J., Zha, Y. Y., Wang, J. J., Liu, M. W., and Hao, Y. H. (2019). "Onset of suffusion in upward seepage under isotropic and anisotropic stress conditions." *Eur. J. Environ. Civ. Eng.*, 23(12), 1520–1534.

Marot, D., Le, V. D., Garnier, J., Thorel, L., and Audrain, P. (2012). "Study of scale effect in an internal erosion mechanism: centrifuge model and energy analysis." *Eur. J. Environ. Civ. Eng.*, 16(1), 1–19.

Ovalle-Villamil, W. and Sasanakul, I. (2020). "Assessment of centrifuge modelling of internal erosion induced by upward flow conditions." *Int. J. Phys. Model. Geotech.*, 21(5), 251–267.

Rochim, A., Marot, D., Sibille, L., and Le, V. T. (2017). "Effects of hydraulic loading history on suffusion susceptibility of cohesionless soils." *J. Geotech. Geoenviron. Eng.*, 143(7), 04017025.

Skempton, A. W. and Brogan, J. M. (1994). "Experiments on piping in sandy gravels." *Géotechnique*, 44(3), 449–460.

Slangen, P. (2015). "On the influence of effective stress and micro-structure on suffusion and suffosion." Ph.D. thesis, University of British Columbia, Vancouver, Canada.

Stevenson, R. E. (2024). "Hydromechanical factors influencing seepage-induced suffusion in internally unstable soils." Ph.D. thesis, University of Sheffield, Sheffield, U.K.

Taylor, R. (1994). *Geotechnical centrifuge technology*. Cambridge: CRC Press.

Thusyanthan, N. I. and Madabhushi, S. P. G. (2003). *Scaling of Seepage flow velocity in centrifuge models*. CUED/D-SOILS/TR326.

Wan, C. and Fell, R. (2008). "Assessing the potential of internal instability and suffusion in embankment dams and their foundations." *J. Geotech. Geoenviron. Eng.*, 134, 401–407.

Zhong, C., Le, V. T., Bendahmane, F., Marot, D., and Yin, Z. Y. (2018). "Investigation of spatial scale effects on suffusion susceptibility." *J. Geotech. Geoenviron. Eng.*, 144(9), 014018067.

List of Tables

TABLE 1. Centrifuge scaling laws relating to the phenomenon of suffusion (quantities marked † are discussed in the text)

Parameter	Scaling Factor (prototype/model)
Length	N
Pressure	1
Stress σ	1
Density ρ	1
Gravitational acceleration g	N
Seepage velocity v	N
† Darcy's permeability k	N
† Hydraulic gradient i	1

TABLE 2. Overview of centrifuge testing parameters and global permeability results. *indicates the increase in δh_{CHT} alternated for each interval due to apparatus limitations

Test	T40L2.5	T40L2.5(R)	T40S2.5	T30L2.5/5	T20L5	T10L10
g-level, N	40	40	40	30	20	10
# stages	3	2	4	3	2	2
σ'_{vm0} (kPa)	117.1	117.4	69.5	88.5	66.8	29.3
δh_{CHT} (mm)	2.5	2.5	2.5	2.5 / 5*	5	10
Increment duration (s)	120	120	120	120	120	600
$EG_{app,final}$ (kPa/m)	196.5	285.8	480.7	154.1	138.8	61.6
$k_{1g,initial}$ ($\times 10^{-5}$ m/s)	1.43	1.60	1.50	2.47	2.85	1.51
Δk_{1g} (%)	+42.1	+23.7	+12.1	-20.2	-43.4	-21.6
Global suffusion?	Yes	Yes	Yes	Yes	No	No

List of Figures

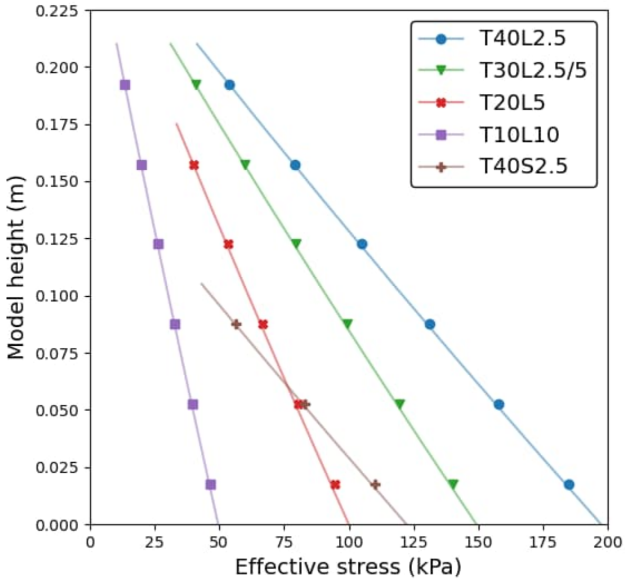

(a) Calculated effective stress profiles within the specimens at the onset of seepage flow (estimated values)

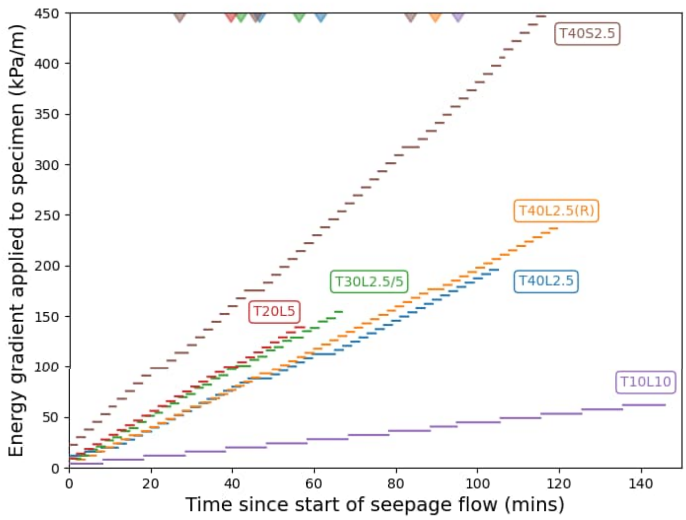

(b) Hydraulic loading regimes with centrifuge spin-down breaks marked by colour coded arrows on the top boundary.

Fig. 1. Hydromechanical loading regimes applied in this study.

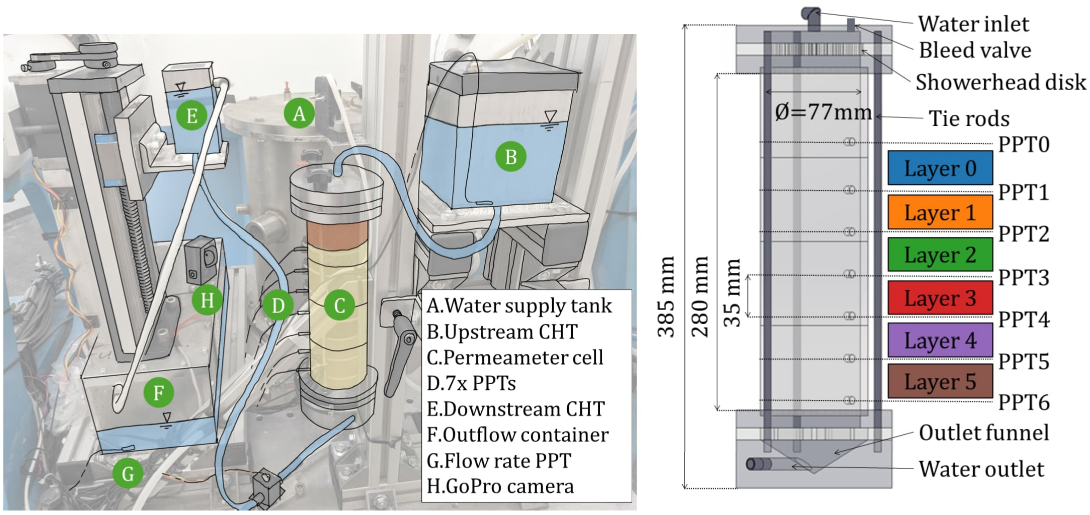

(a) Centrifuge payload **(b)** Permeameter cell

Fig. 2. Novel centrifuge permeameter apparatus with key components identified

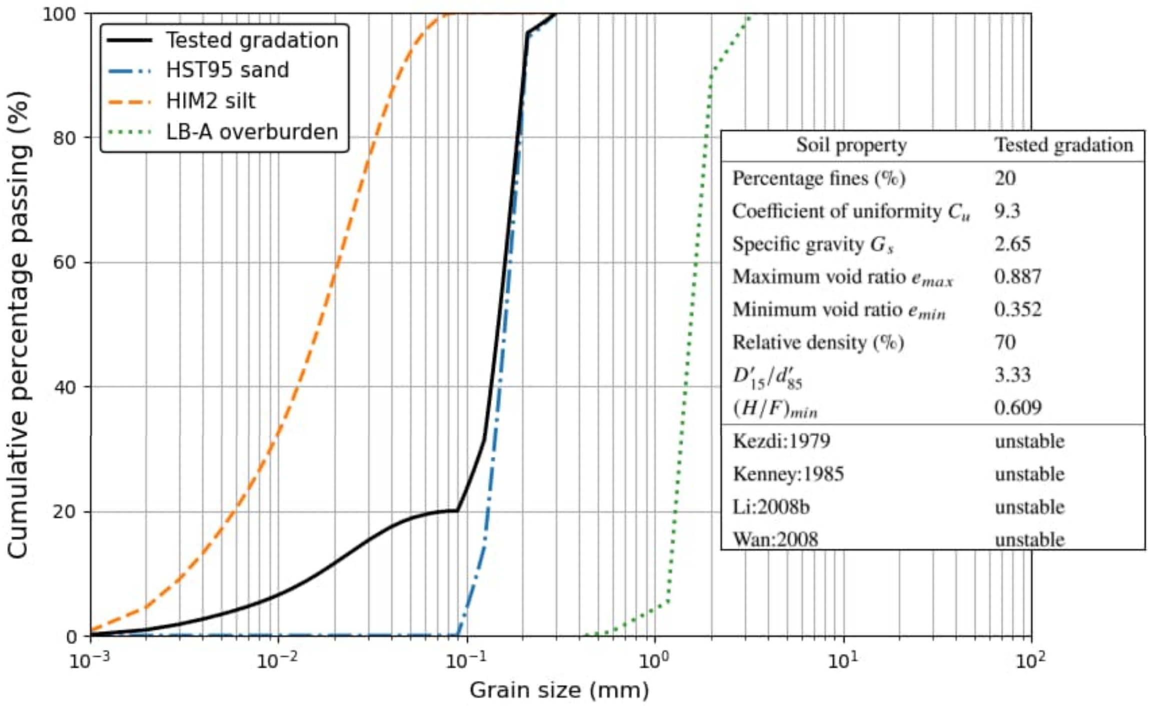

Soil property	Tested gradation
Percentage fines (%)	20
Coefficient of uniformity C_u	9.3
Specific gravity G_s	2.65
Maximum void ratio e_{max}	0.887
Minimum void ratio e_{min}	0.352
Relative density (%)	70
D'_{15}/d'_{85}	3.33
$(H/F)_{min}$	0.609
Kezdi:1979	unstable
Kenney:1985	unstable
Li:2008b	unstable
Wan:2008	unstable

Fig. 3. Particle size distributions of the constituent soils and the tested unstable soil mix

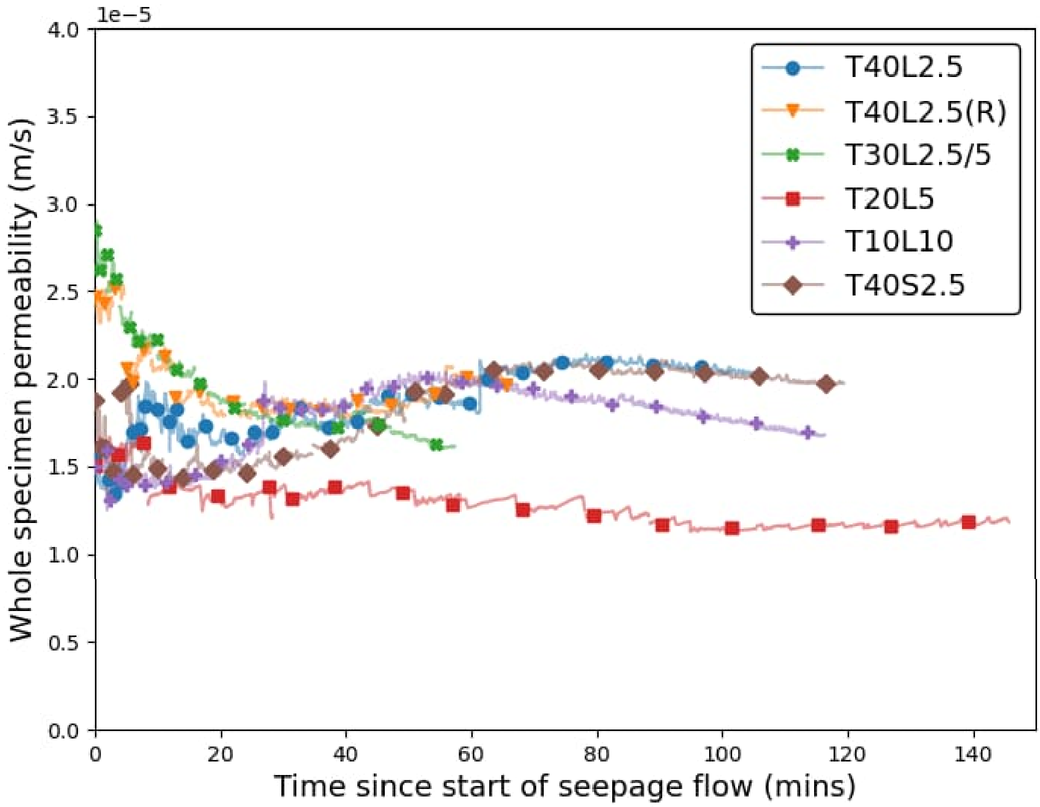

Fig. 4. The evolution of global permeability over the test duration for each centrifuge test

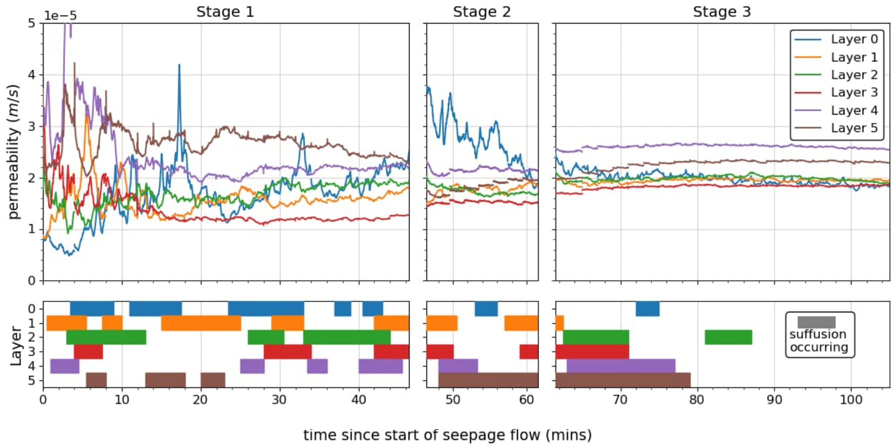

(a) T40L2.5

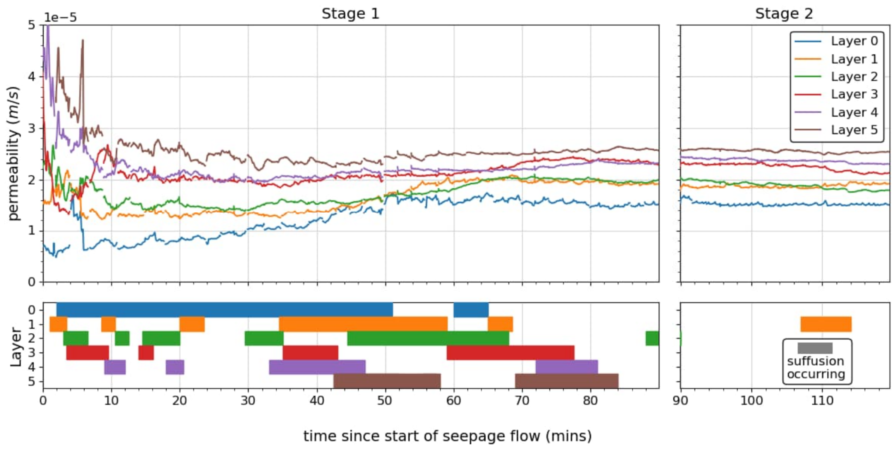

(b) T40L2.5(R)

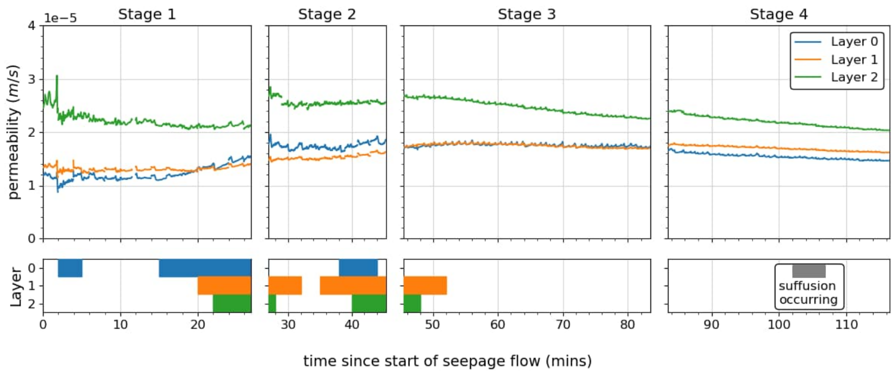

(c) T40S2.5

Fig. 5. The evolution of layer permeability over the test duration with a timeline of suffusion events in each layer for tests conducted at 40-g

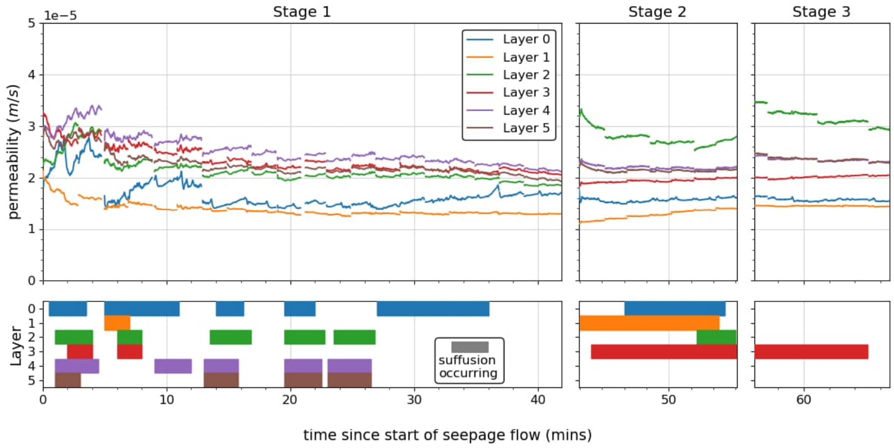

(a) T30L2.5/5

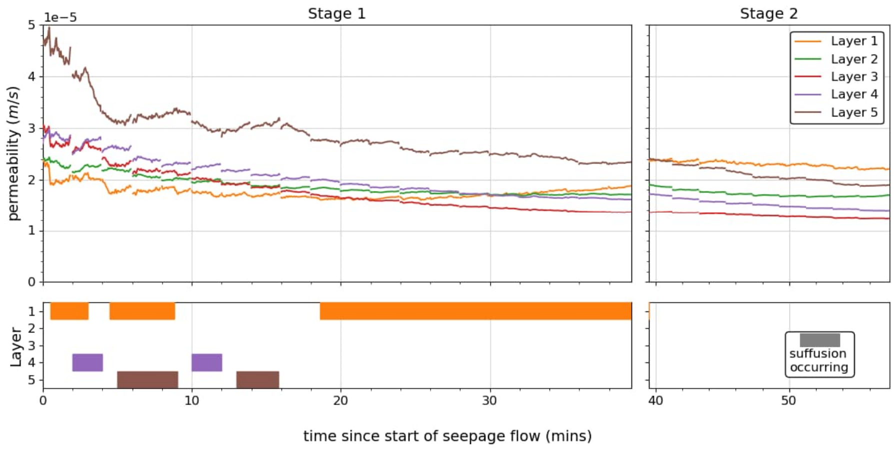

(b) T20L5

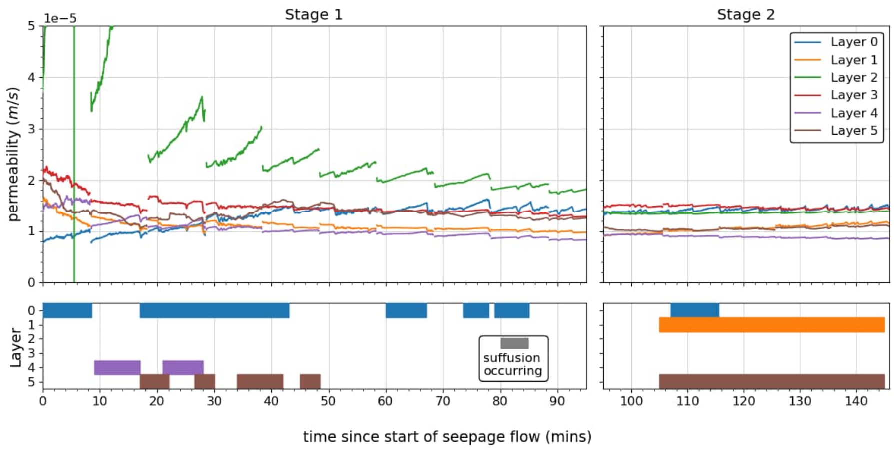

(c) T10L10

Fig. 6. The evolution of layer permeability over the test duration with a timeline of suffusion events in each layer for tests conducted at lower than 40-g

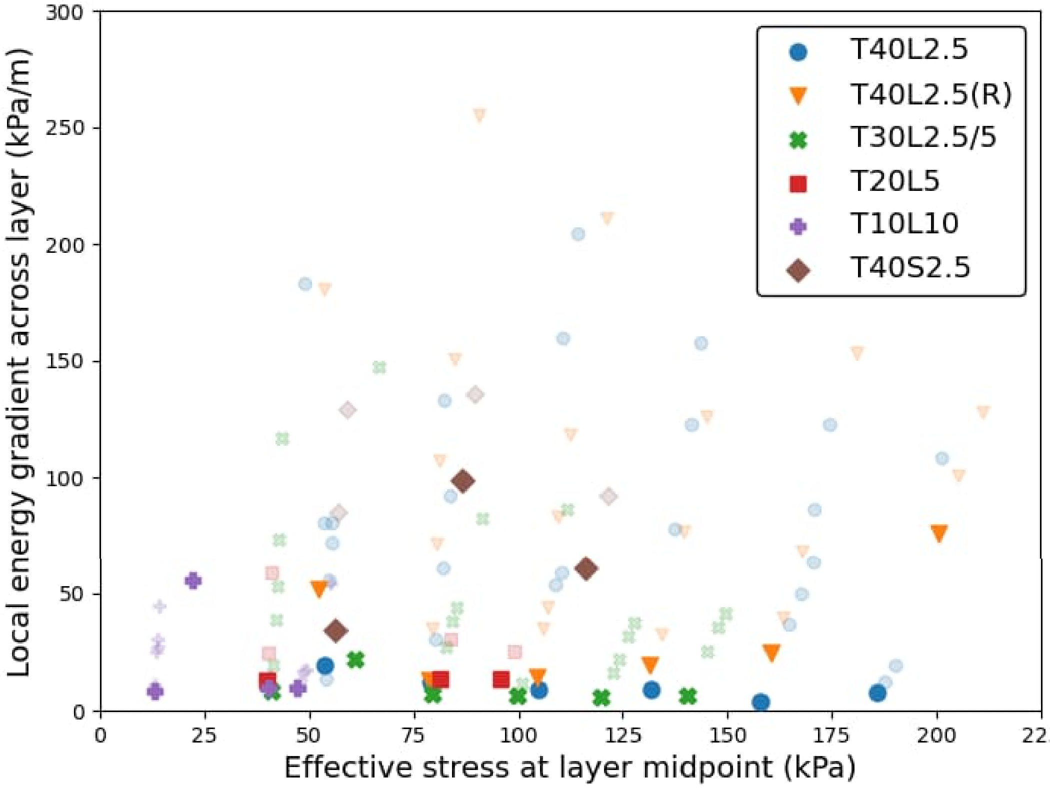

Fig. 7. Energy gradient and effective stress level in each layer at the first onset of a suffusion event in each layer of the centrifuge tests

Figure 1 a

Click here to access/download;Figure;1a_effective_stress_profile.tiff

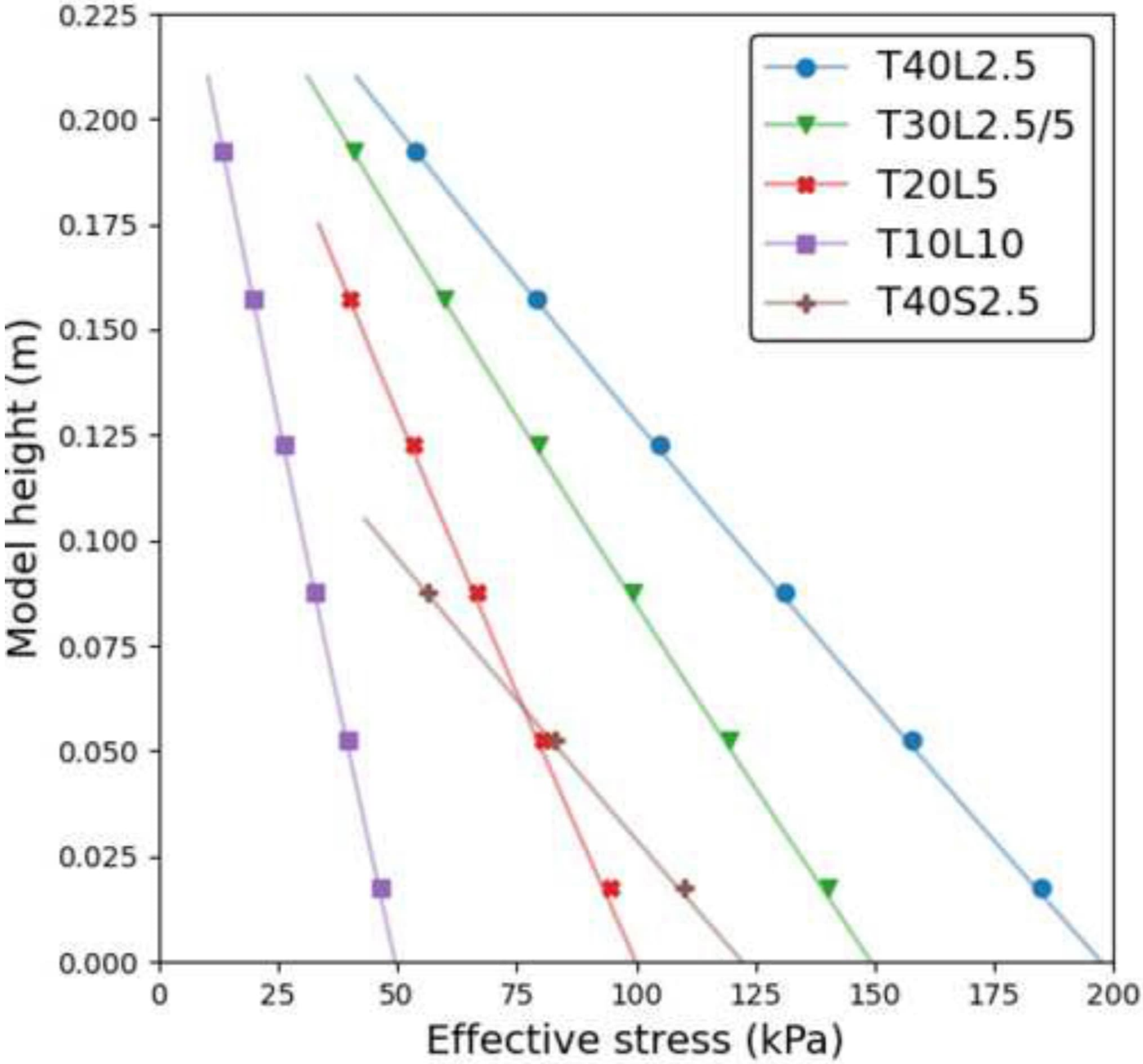

Figure 1 b

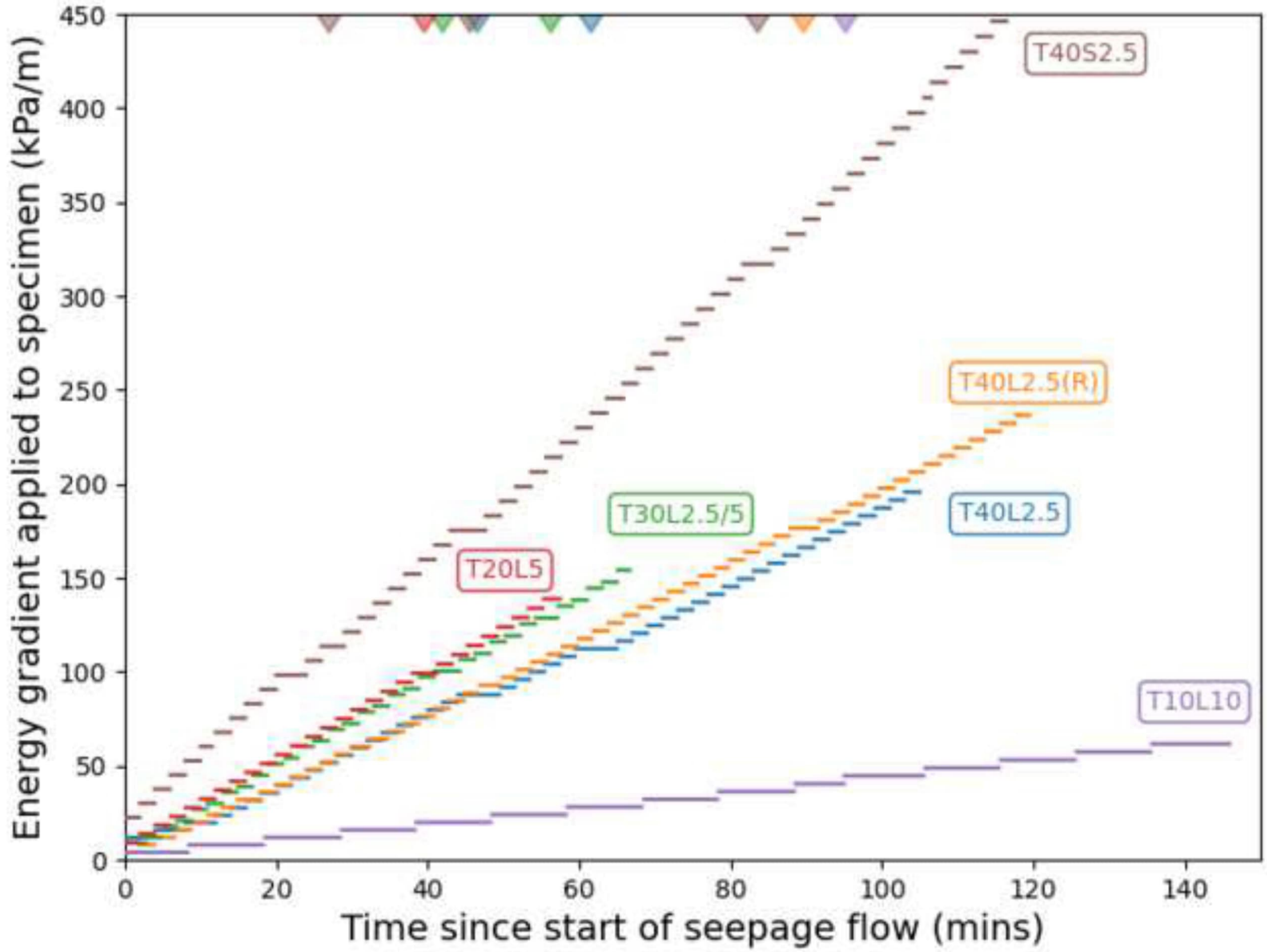
Energy gradient applied to specimen (kPa/m)
0
50
100
150
200
250
300
350
400
450
Time since start of seepage flow (mins)
0
20
40
60
80
100
120
140
T40S2.5
T40L2.5(R)
T40L2.5
T30L2.5/5
T20L5
T10L10

Figure 2 a

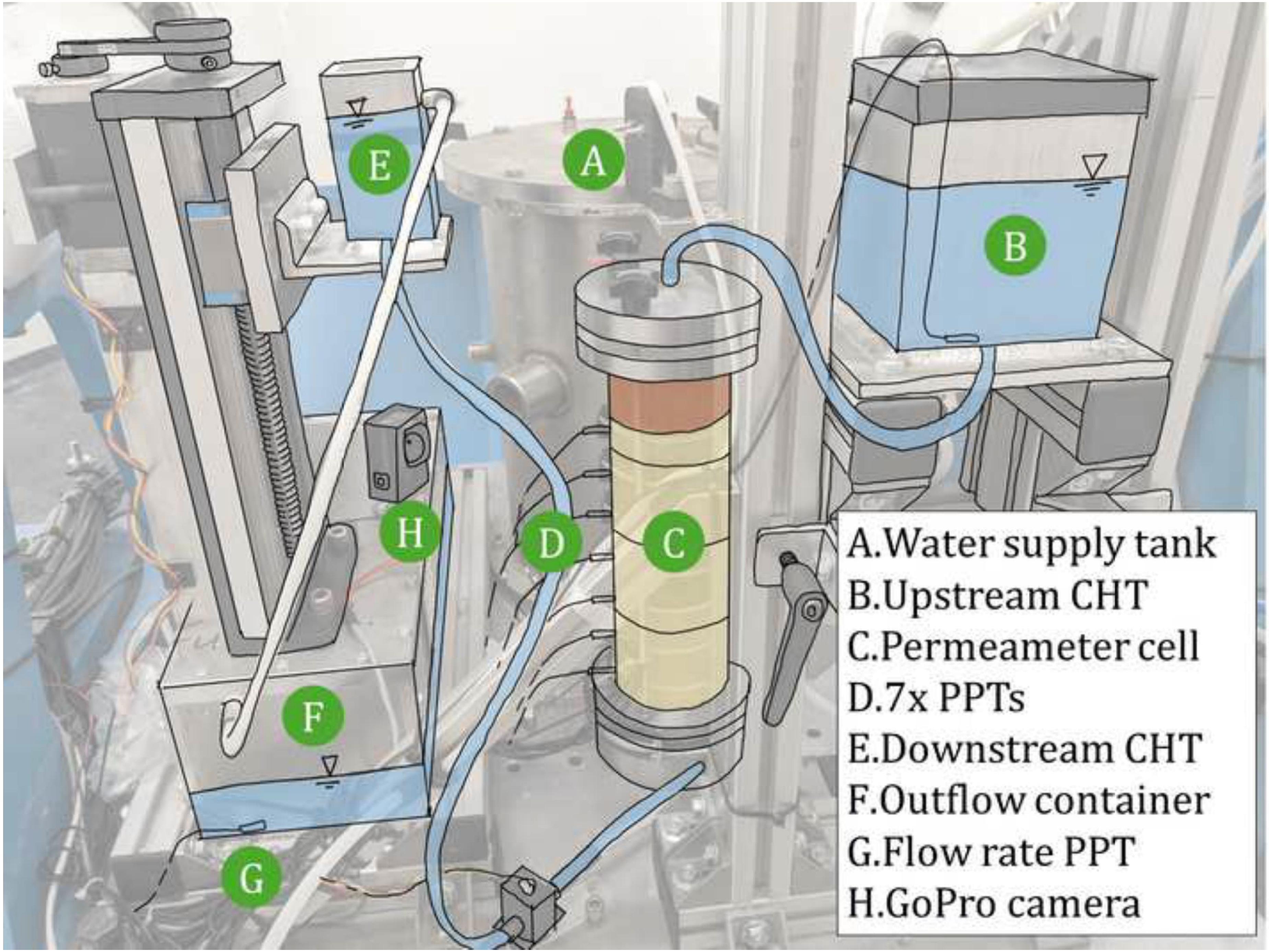
A
B
C
D
E
F
G
H
A.Water supply tank
B.Upstream CHT
C.Permeameter cell
D.7x PPTs
E.Downstream CHT
F.Outflow container
G.Flow rate PPT
H.GoPro camera

Figure 2 b

Click here to access/download;Figure;2b_permeameter_cell.tif

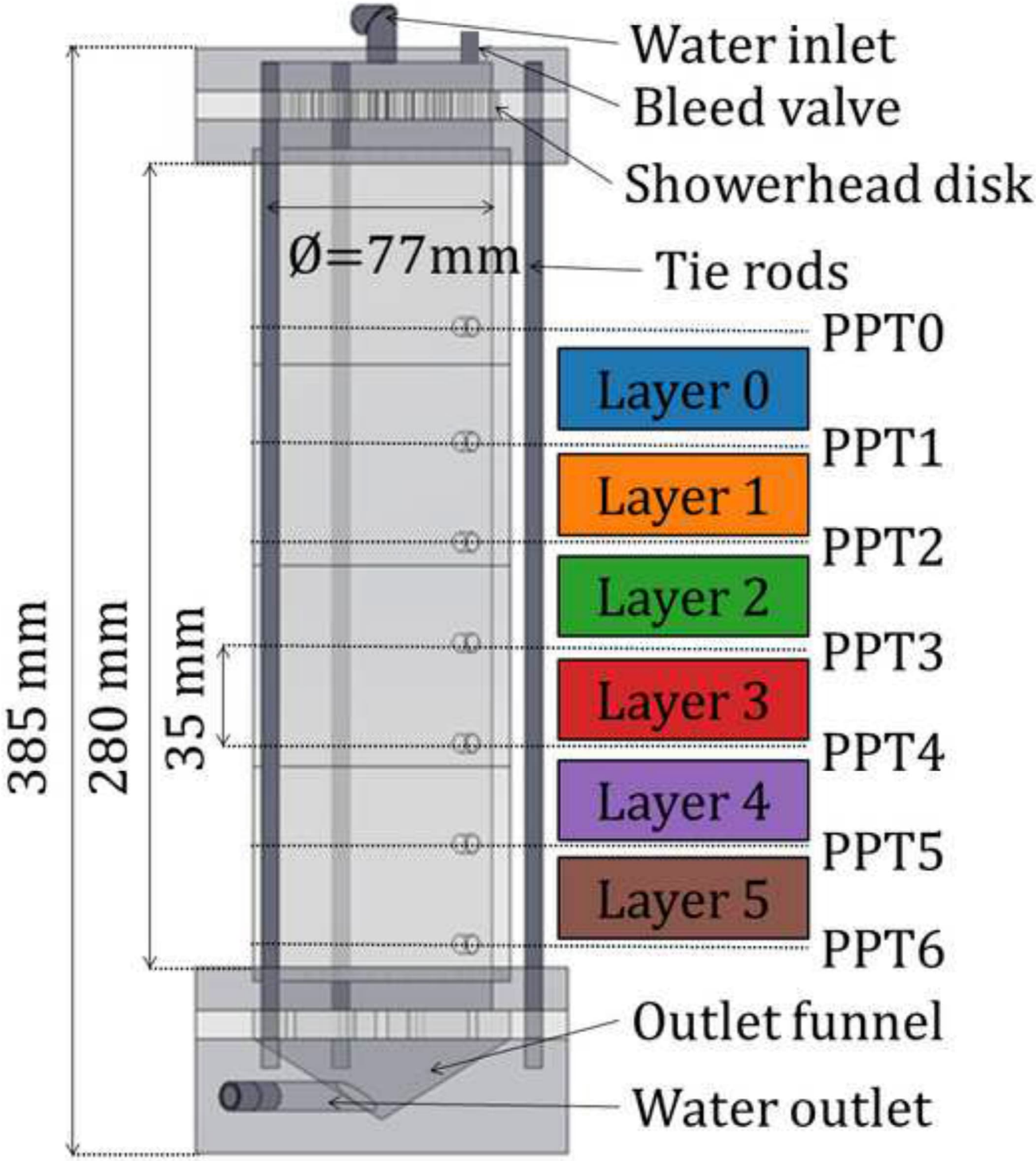

Figure 3

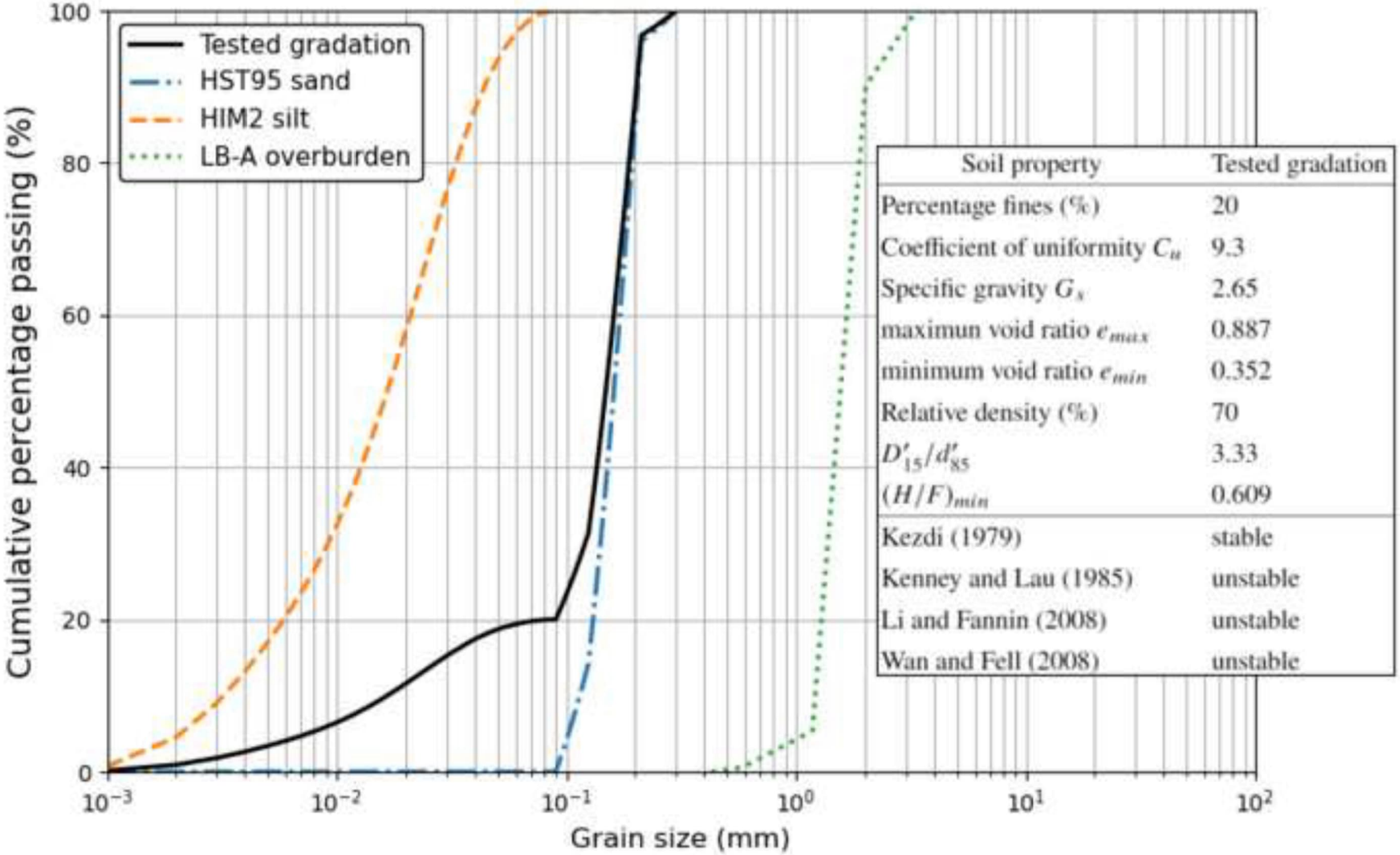

Soil property	Tested gradation
Percentage fines (%)	20
Coefficient of uniformity C_u	9.3
Specific gravity G_s	2.65
maximun void ratio e_{max}	0.887
minimum void ratio e_{min}	0.352
Relative density (%)	70
D'_{15}/d'_{85}	3.33
$(H/F)_{min}$	0.609
Kezdi (1979)	stable
Kenney and Lau (1985)	unstable
Li and Fannin (2008)	unstable
Wan and Fell (2008)	unstable

Figure 4

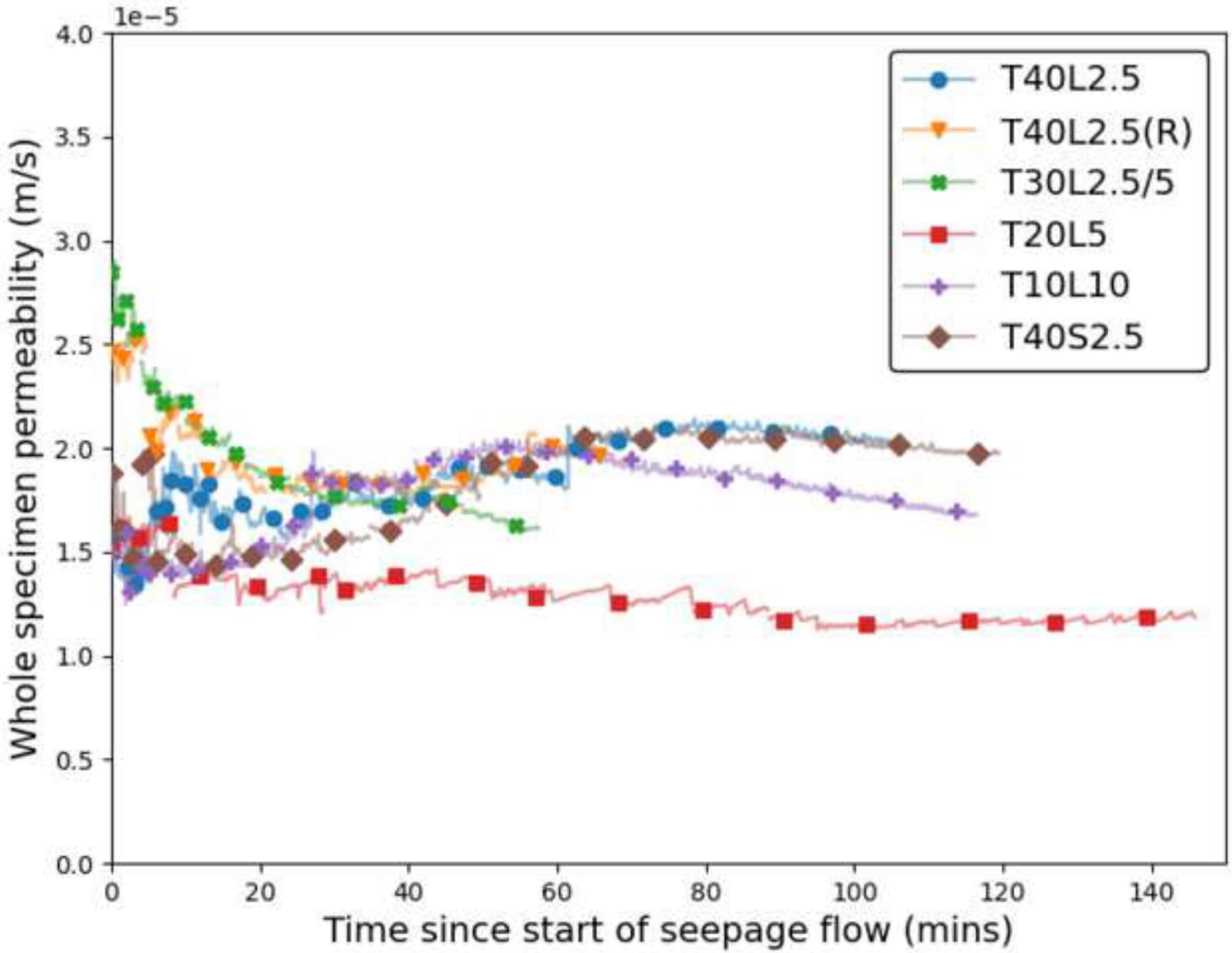
1e−5
Whole specimen permeability (m/s)
4.0
3.5
3.0
2.5
2.0
1.5
1.0
0.5
0.0
0
20
40
60
80
100
120
140
Time since start of seepage flow (mins)
T40L2.5
T40L2.5(R)
T30L2.5/5
T20L5
T10L10
T40S2.5

Figure 5 a

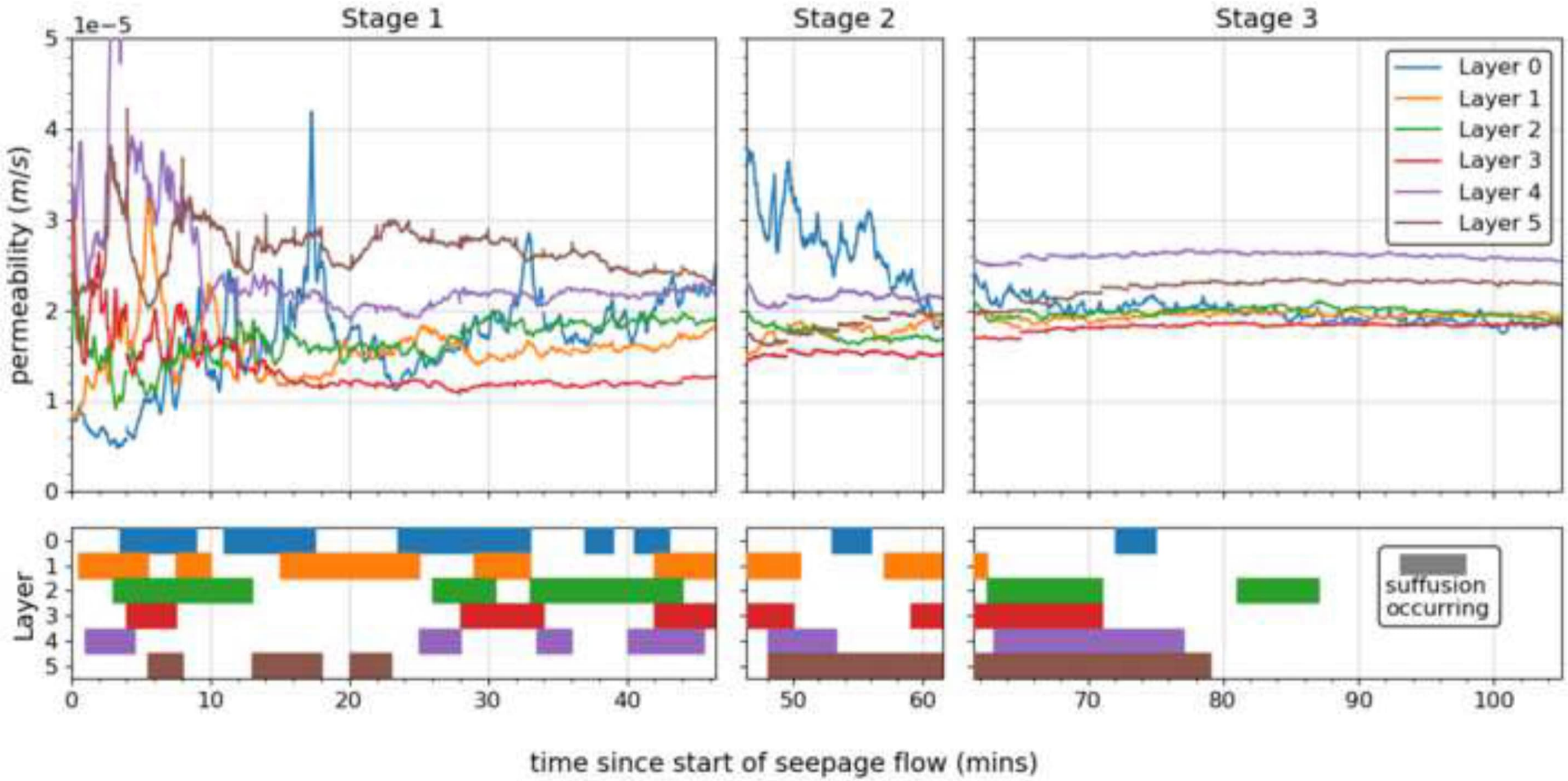
Stage 1
Stage 2
Stage 3
1e−5
permeability (m/s)
Layer 0
Layer 1
Layer 2
Layer 3
Layer 4
Layer 5
Layer
suffusion occurring
time since start of seepage flow (mins)

Figure 5 b

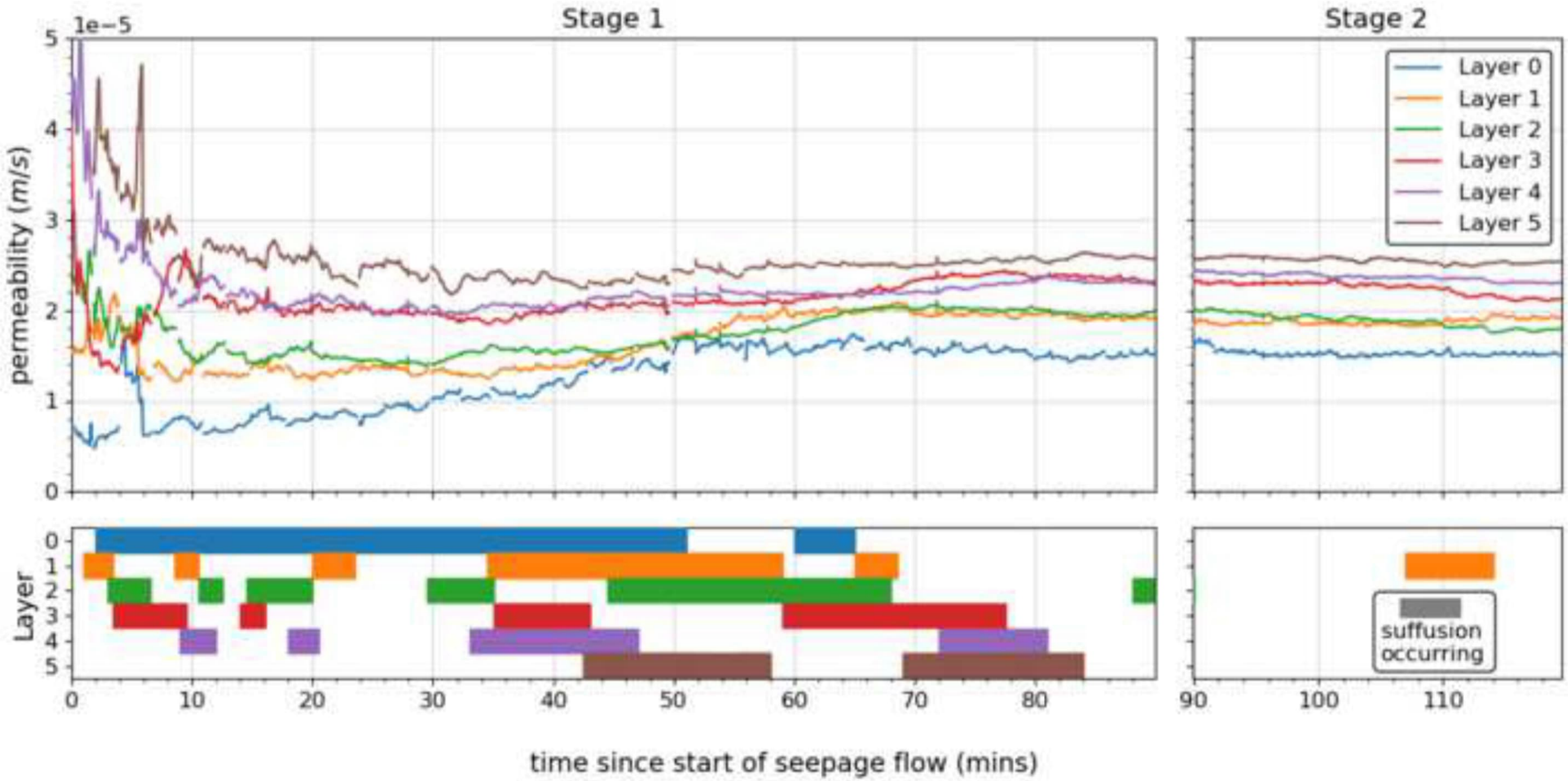

Stage 1
Stage 2
1e−5
permeability (m/s)
5
4
3
2
1
0
Layer 0
Layer 1
Layer 2
Layer 3
Layer 4
Layer 5
Layer
0
1
2
3
4
5
suffusion occurring
0
10
20
30
40
50
60
70
80
90
100
110
time since start of seepage flow (mins)

Figure 5 c

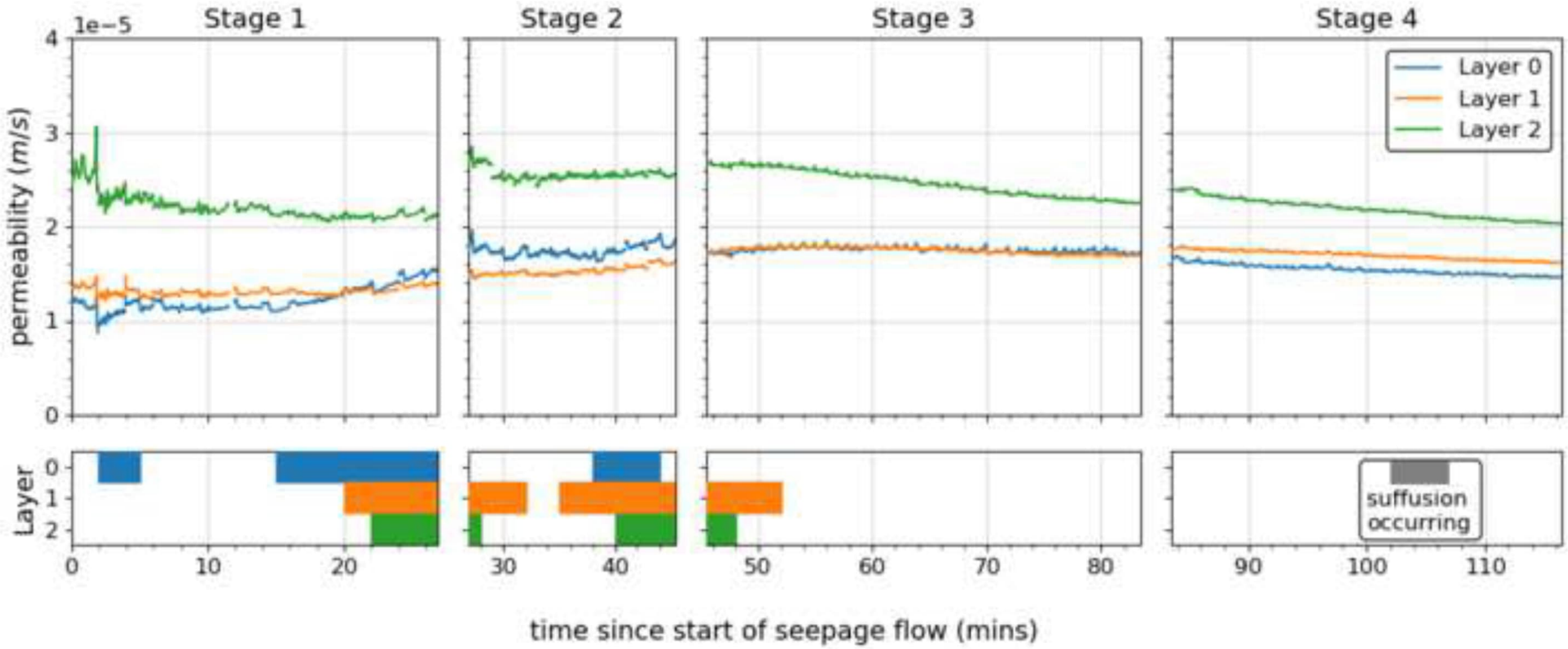

Stage 1
Stage 2
Stage 3
Stage 4
1e−5
permeability (m/s)
Layer 0
Layer 1
Layer 2
Layer
suffusion occurring
time since start of seepage flow (mins)

Figure 6 a

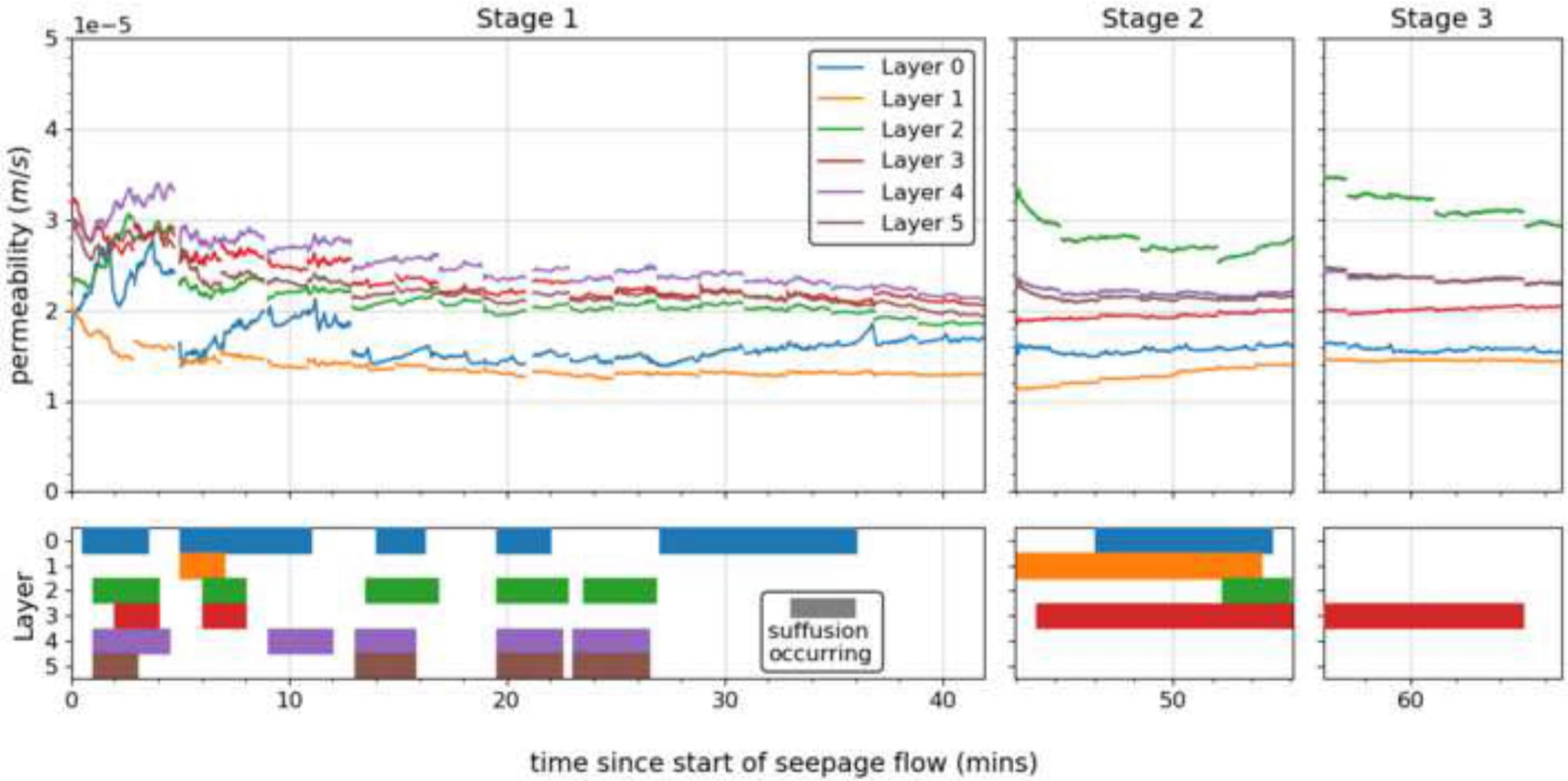
Stage 1
Stage 2
Stage 3
1e−5
permeability (m/s)
Layer 0
Layer 1
Layer 2
Layer 3
Layer 4
Layer 5
Layer
suffusion occurring
time since start of seepage flow (mins)

Figure 6 b

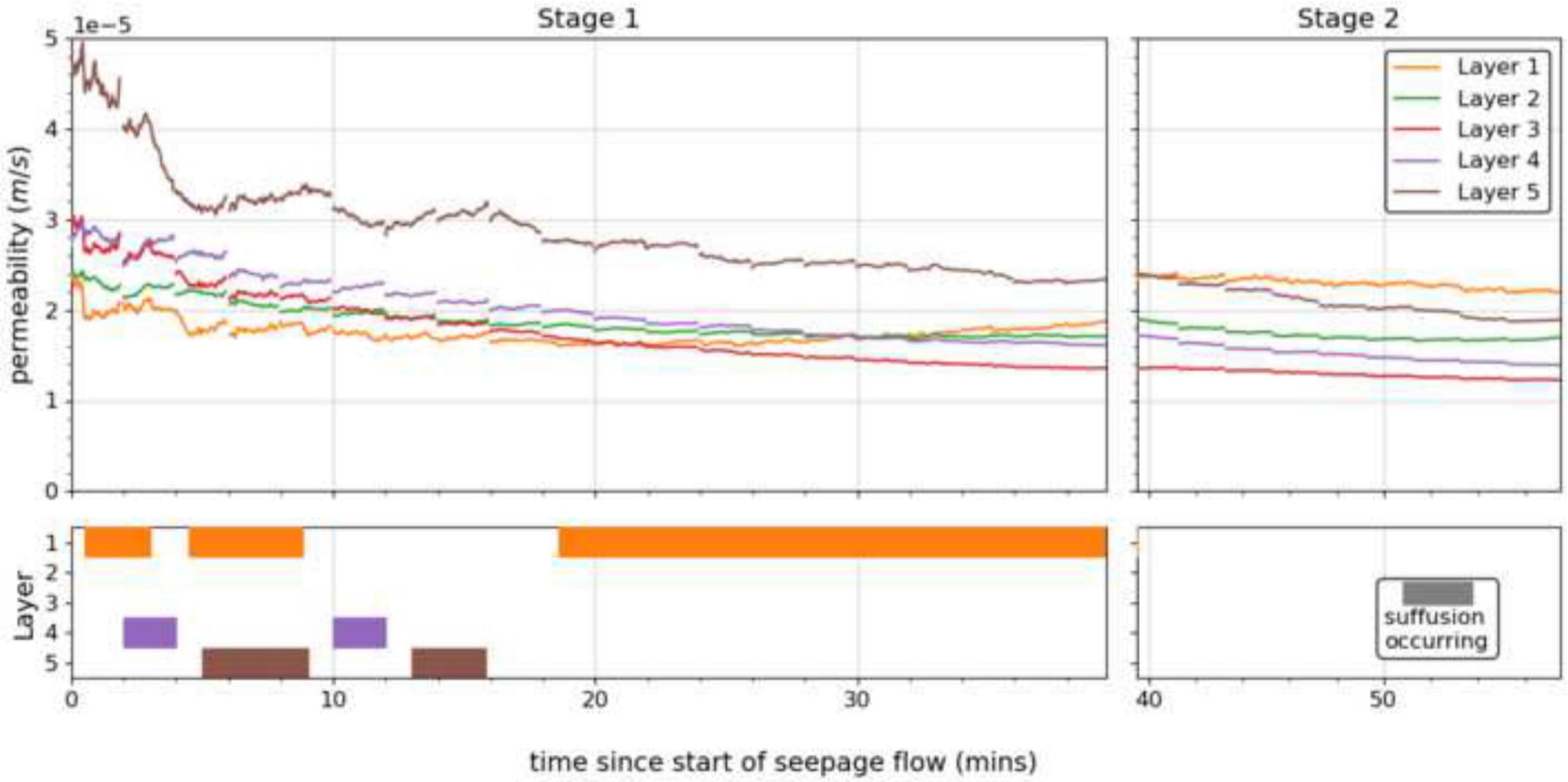

Stage 1
Stage 2
1e−5
permeability (m/s)
5
4
3
2
1
0
Layer 1
Layer 2
Layer 3
Layer 4
Layer 5
Layer
suffusion occurring
0
10
20
30
40
50
time since start of seepage flow (mins)

Figure 6 c

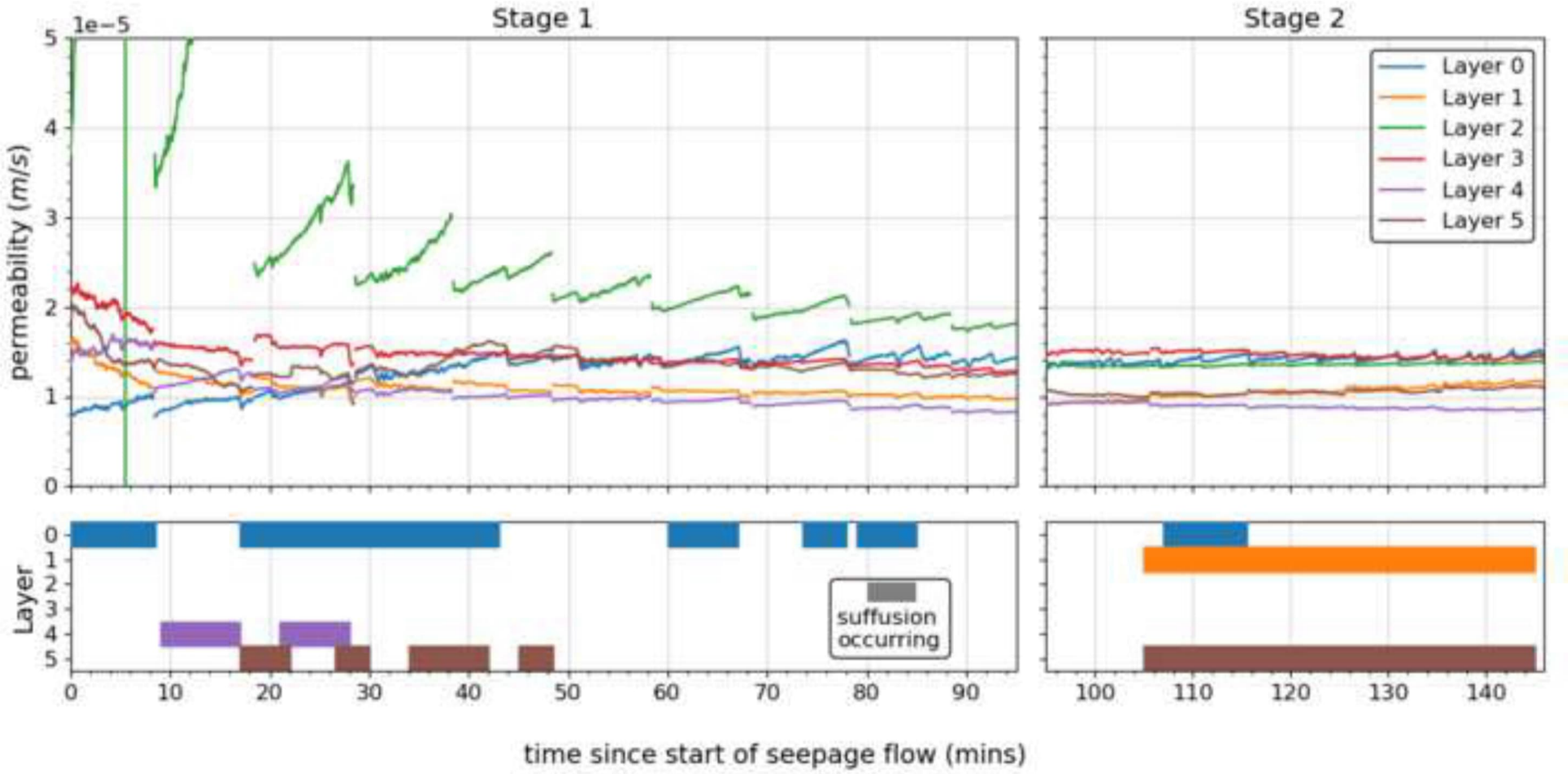
Stage 1
Stage 2
1e−5
permeability (m/s)
5
4
3
2
1
0
Layer 0
Layer 1
Layer 2
Layer 3
Layer 4
Layer 5
Layer
suffusion occurring
0
10
20
30
40
50
60
70
80
90
100
110
120
130
140
time since start of seepage flow (mins)

Figure 7

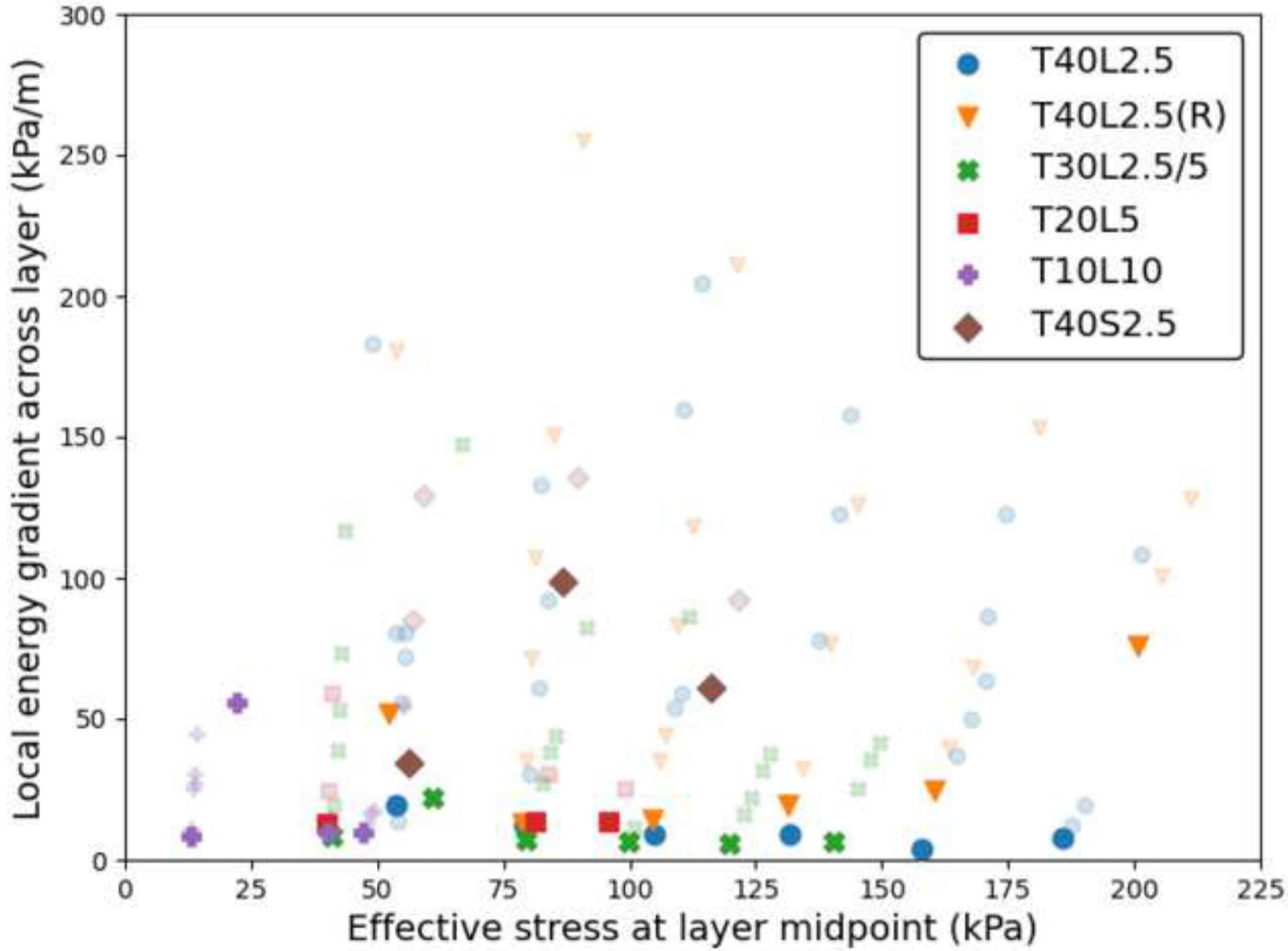

Local energy gradient across layer (kPa/m)
300
250
200
150
100
50
0
0
25
50
75
100
125
150
175
200
225
Effective stress at layer midpoint (kPa)
T40L2.5
T40L2.5(R)
T30L2.5/5
T20L5
T10L10
T40S2.5

Figures Caption List

Fig. 1. Hydromechanical loading regimes applied in this study.

a) Calculated effective stress profiles within the specimens at the onset of seepage flow (estimated values).

b) Hydraulic loading regimes with centrifuge spin-down breaks marked by colour coded arrows on the top boundary.

Fig. 2. Novel centrifuge permeameter apparatus with key components identified.

a) Centrifuge payload.

b) Permeameter cell.

Fig. 3. Particle size distributions of the constituent soils and the tested unstable soil mix.

Fig. 4. The evolution of global permeability over the test duration for each centrifuge test.

Fig. 5. The evolution of layer permeability over the test duration with a timeline of suffusion events in each layer for tests conducted at 40-g.

a) T40L2.5

b) T40L2.5(R)

c) T40S2.5

Fig. 6. The evolution of layer permeability over the test duration with a timeline of suffusion events in each layer for tests conducted at lower than 40-g.

a) T30L2.5/5

b) T20L5

c) T10L10

Fig. 7. Energy gradient and effective stress level in each layer at the first onset of a suffusion event in each layer of the centrifuge tests.

Supplemental Materials File

Click here to access/download
Supplemental Materials File
GTENG - 13169 Supplemental Materials.pdf